8-2014

Photomechanical actuation of liquid crystal nanotube elastomers.

Xiaoming Fan
University of Louisville

PHOTOMECHANICAL ACTUATION OF LIQUID CRYSTAL NANOTUBE ELASTOMERS

By

Xiaoming Fan
B.Eng., Beijing University of Chemical Engineering, 2007

A Thesis
Submitted to the Faculty of the
J. B. Speed School of Engineering of the University of Louisville
in Partial Fulfillment of the Requirements
for the Degree of

Master of Science

Department of Mechanical Engineering
University of Louisville
Louisville, Kentucky

August 2014

PHOTOMECHANICAL ACTUATION OF LIQUID CRYSTAL

NANOTUBE ELASTOMERS

By

Xiaoming Fan

B.Eng., Beijing University of Chemical Engineering, 2007

A Thesis Approved On

July 11, 2014

by the following Thesis Committee :

Dr. Balaji Pachapakesan, Thesis Director

Dr. Robert W. Cohn

Dr. Stuart J. Williams

ACKNOWLEDGEMENTS

I would like to thank Dr. Baloo for his great help and support throughout the project. Thanks as well to the Small Systems Lab members, Dr. Jarro Carlos, Farhad Khosravi, Loeian Masoud, and especially Ben King and Dr. James Loomis whom I collaborated extensively on the order parameter calculation and composites fabrication processes.

Dr. Roger D. Bradshaw, Dr. Jacek B. Jasinski and Dr. Tereza Paronyan provided invaluable advice and instrument support. Numerous other researchers and staff at U of L provided valuable contributions as well.

I am grateful to my wife Wuyu Zhang and my baby son Samuel Fan, for all their love and encouragement.

ABSTRACT

PHOTOMECHANICAL ACTUATION OF LIQUID CRYSTAL

NANOTUBE ELASTOMERS

Xiaoming Fan

July 11, 2014

Elastomeric composites based on nanotube liquid crystals (LCs) that preserve the internal orientation of nanotubes could lead to anisotropic physical properties and flexible energy conversion. Using simple vacuum filtration technique of fabricating nanotube LCs films and utilizing a transfer process to poly (dimethyl) siloxane wherein the LCs arrangement is preserved, in this thesis we demonstrate unique and reversible photomechanical response of this layered composite to excitation by near infra-red (NIR) light at ultra-low nanotube mass fractions. Schlieren textures were noted in these LCs composites confirming long range macroscopic nematic order of nanotubes within the composites. Maximum photomechanical stress of ~23kPa, energy conversion factor of 0.5 MPa/W and energy conversion of ~0.0045% was achieved. The combination of properties, namely, optical anisotropy, reversible mechanical response to NIR excitation and flexible energy conversion all in one system makes nanotube LCs elastomers important for soft photochromic actuation, energy conversion and photo-origami applications.

TABLE OF CONTENTS

LIST OF FIGURES

PAGE

CHAPTER 1

INTRODUCTION

Materials that flow like liquids and yet can order themselves macroscopically like crystals are called liquid crystals (LCs) and hold great technological and commercialization potential[1]. LCs can also be found in nature, such as tobacco mosaic virus[2], proteins[3] and cells[4, 5]. Modern day applications of LCs include polymers such as Kevlar for bullet proof jackets[6], and electro-optics in digital and computer displays[7, 8]. The uniqueness of LCs is their tendency to align in specific directions with macroscopic and long range ordering. In recent years, with the synthesis of nanotube LCs by Windle et al.,[9] organization of nanotubes as LCs has become an interesting and attractive area of study to realize low cost commercial applications based on self-aligned nanotubes. LCs nematic self-assembly of nanotubes, as well as graphene and other 2-D nanomaterials, presents opportunities in developing novel macroscopic composites with long range order and unique anisotropic properties. Energy efficient photo-mechanical systems based on nanotube LCs-elastomers that combine anisotropic optical and thermal properties of the nanotube LCs and elasticity of the polymer network are yet to be explored. In the recent past, Ben King *et al*., reported LC of carbon nanotube films using simple vacuum filtration and their subsequent applications as high performance transistors[10]. Thin films of nanotube LCs with order parameters ranging from S=0.1-0.5 were patterned into conducting channels of transistor devices which showed high on/off ratios ~20,000 and electron mobility values up to μ_e = 79 cm^2/Vs, hole mobility

values up to μ_h = 287 cm2/Vs[10]. In this thesis we demonstrate elastomeric composites based on ultra-small amounts of single wall nanotubes (SWNTs) LCs films in poly (dimethyl) siloxane (PDMS) with high orientational order, optical anisotropy, reversible and macroscopic mechanical response to near infra-red (NIR) excitation. Further, we report strain dependent flexible energy conversion based on change in microscopic order parameters of nanotubes and stress to nanotube mass ratio larger than all the nanotube/graphene based nanocomposite based light driven actuators reported to date[11-13]. The amount of nanotube used in this work is also ~10,000 times smaller than past reported electro-mechanical actuators based on nanotube-polymer composites[14], suggesting the high importance of spontaneous nanotube order for low cost commercial applications. Further, the methods used here may enable standardization of nanotube-composite fabrication processes in general, the lack of which has hindered commercialization.

The underlying reasons for this investigation into carbon nanotubes-based liquid crystal composites are: (1) Carbon nanotubes are efficient at light absorption and subsequent energy transduction to polymeric chains, thus enabling resulting composites to undergo photo-mechanical actuation. (2) LCs carbon nanotubes introduce improved mechanical properties to the PDMS matrix. Hence, evaluation of differences in resulting photo mechanical properties between aligned carbon nanotubes and randomly oriented carbon nanotubes will allow for creation of application-specific composites. (3) Conductive properties of carbon nanotubes can be used to introduce sensing properties into the composites, resulting in the ability to sense and actuate in a single solid state material. (4) LCs structure could realize low cost commercial applications based on self-

aligned technology. (5) Use of LCs carbon nanomaterials in general is still in its infancy, and therefore of enormous scientific interest. (6) Perhaps most importantly, the LCs carbon nanotubes with different order parameter influences the photomechanical actuation stress, energy conversion efficiency making it research interesting from both science and application aspects.

CHAPTER 2

BACKGROUND

2.1 Carbon Nanotubes

Carbon is the 15th most abundant element in the Earth's crust, and the fourth most abundant element in the universe by mass[15]. It plays a very important rules as a fundamental building block of intelligent life[16]. There are several *allotropes* of carbons of which the best known are graphite, diamond and amorphous carbon. From the beginning of human history, graphite and diamond were the only two known carbon allotropes[17]. In the last few decades of 20^{th} century, in addition of the discovery of synthetic carbon forms have expanded the carbon allotropes families. These carbon allotropes include buckyballs[18], nanotubes[19], and graphene[20].

As early as 1952, Radushkevich and Lukyanovich publish a paper in the Soviet Journal of Physical Chemistry predicting hollow graphitic carbon fibers that are 50 nanometers in diameter[21]. However, it took almost 40 years until the first observation of the carbon nanotubes. In 1991, carbon nanotubes were discovered in the soot of arc discharge at NEC, by Japanese researcher Sumio Iijima[19]. In 1993, groups led by Donald S. Bethune at IBM[22] and Sumio Iijima at NEC[23] independently discover single-wall carbon nanotubes and methods to produce it using transition-metal catalysts

Generally, carbon nanotubes could be classified to sing-walled nanotubes (SWNTs) and multi-walled nanotubes (MWNTs). SWNTs are hollow 1D tubes of carbon atoms with nanometer diameters and lengths in the micron range, while MWNTs can be thought of as two or more concentric SWNTs[19]. The chemical bonding of carbon nanotubes is composed entirely of sp^2 bonds. These bonds are stronger than the sp^3 bonds found in alkanes and diamond, provide nanotubes with their extraordinary thermal conductivity and mechanical and electrical properties[24]. SWNTs are an important variety of carbon nanotube because their band gap can vary from zero to about 2 eV and their electrical conductivity can show metallic or semiconducting behavior[25, 26]. In the past two decades, the magic cylindrical nanostructure has attracted a lot of research interest and could potential applied to structural reinforcement[27], electrical circuits[28], electrical cables and wires[29], paper batteries[30], solar cells[31], hydrogen storage[32], supercapacitor[33], radar absorption[34], medical[35], acoustics[35] and actuators[12-14].

2.2 Photo-mechanical Actuation

Materials that can undergo a change in dimensions under the application of external energy thereby performing useful work are used as actuators in modern technology. Modern day actuators include electromagnetic motors, hydraulic actuators, pneumatic actuators, shape memory alloys, electro-active polymers, peizoelectrics and magnetic actuators[36].

In recent years, a class of light driven actuators has been developed. Light as a form of energy to drive actuators has several advantages including clean energy, control

of number of photons and wireless/remote energy transfer[12, 37]. However, unlike electro-mechanical actuators, light driven actuators are not common. The reason is due to lack of materials to transduce light energy into mechanical energy to elicit a macroscopic photo-mechanical response. However, in recent years, this field is progressing rapidly with soft materials and new composites based on nanomaterials.

Photo-mechanical actuation has been achieved in benzeazone liquid crystal elastomers and their hybrids, poly vinylidene di fluoride (PVDF), shape memory polymers, chalcogenide glasses, nanotube-elastomer and more recently graphene-elastomer composites[12, 13, 38-41]. These photomechanical actuators use different principles such as photochromic effects in azobenzenes resulting in reversible molecular alignment on irradiation of UV or visible light, light induced fluidity, diffusion and structural changes as in chalcogenides, pre-programmed deformation through extrusion and thermally assisted recovery above the glass transition temperature as in shape memory polymers, radiation induced heating as in PVDF and fast photothermal mechanism assisted by strong sp^2 and sp^3 covalent bonds in nanotube and graphene based composites.

Pioneering work by Ahir *et al*., [12]showed novel and reversible photomechanical actuation by the addition of nanotubes in PDMS which otherwise would not exist in that system. In the same year, Lu *et al.*, [42]demonstrated a photomechanical actuator using nanotube films and showed stress responses higher than peak capacity of human muscles. The developments in nanotube/polymer systems as photo-actuators are promising due to reversibility of macroscopic mechanical response with NIR light, high strength of composites, actuator strokes of ~2-5%, stresses of tens of kilopascals, percolation dependent NIR mechanical response, ability to adapt to lithography without changing the

configurational state of the polymer and subsequent device manufacturing. More recent work in the area of graphene nanoplatelet (GNP, ~3–5 layer stacks of graphene)-based photo-actuators by Loomis *et al*., [13]has shown an optical-to-mechanical energy conversion factor of 7 MPa/W, reversible actuation, high actuator stresses, saturable absorption, layer and dimensional state dependent mechanical stiffness, low fabrication costs, and ability to integrate with existing commercial electronics and optics.

2.3 Liquid Crystals

Liquid Crystals (LCs) is a stable phase of matter characterized by anisotropic properties without the existence of a 3-D crystal lattice and it is generally lying between the solid and isotropic ("liquid") phase. It can be considered a fourth state of matter following solid, liquid, and gas[43]. Although LCs has several classification methods, we could easily consider LCs molecules possess rod-like, disc-like anisotropic structures. Generally, rod-like LCs shows nematic or smectic phases depending on the degree of the positional order. Like Figure 2.1 (A), the simplest form of nematic phase have only orientational but no positional order. They are free to move but like to point along one particular direction[44]. The smectic phases have one additional degrees of positional order and generally have separate layers within which there is a loss of positional order. (Figure 2.2 (B)). The disc-like LCs normally form ordered columnar phases, which are characterized by stacked columns of molecules[44].

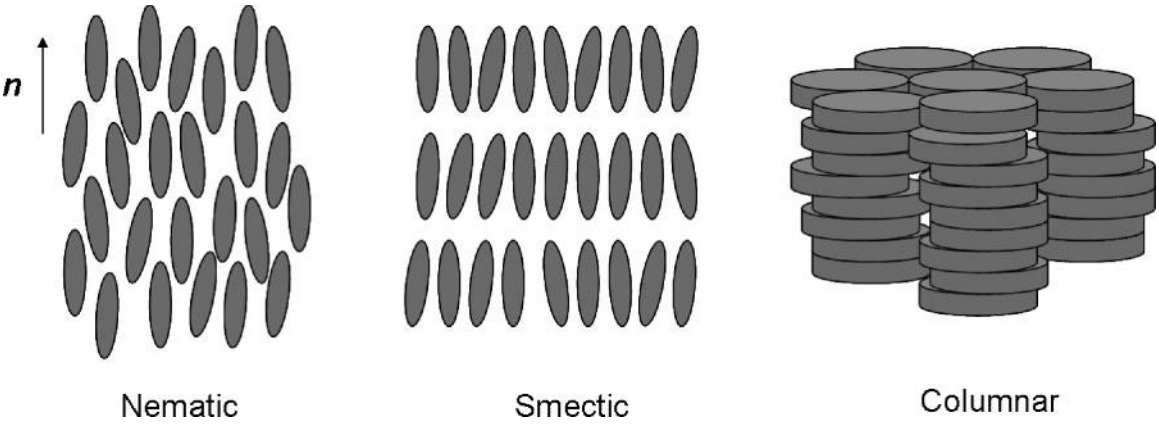

Figure 2.1 | Schematic Image of LCs Structures: nematic, smectic and columnar phases[44]

Carbon nanotubes has large aspect ratio so that it could be a very good example of rod-like liquid crystals. Liquid-crystal phases have been identified in the suspensions (or dispersions) of both MWNTs and SWNTs[9, 45, 46]. Recently, the individual LCs carbon nanotubes has been observed by scanning electron microscopy (SEM)[9, 44]. A lot of interest have been attracted to the LCs carbon nanotubes system.

Carbon nanotubes is a quite complex system, from theoretical viewpoint, strong van der Waals attractions between CNTs must be screened out to form LCs phases at room temperature. This requires a good solvent with an ability to disperse CNTs down to the level of individual tubes. In reality, several methods have been developed to form aligned carbon nanotubes. These include acid oxidation, acid protonation, polymer wrapping, Gradual evaporation, shear flow, vacuum filtration[10, 47-50].

With the remarkable progress in research on CNTs over past several years, nanotubes as LCs materials become more and more important. Control of nanotube alignment has been recognized to play a crucial role in developing the practical

techniques in the exploitation of individual nanotube properties in the macroscopic assemblies. The intrinsic self-assembling nature in the LCs phase is promising in achieving such macroscopic nanotube alignment. As the liquid crystals are highly sensitive to the external forces, the applied fields, such mechanical shear flow, electric or magnetic stimuli, as well as surface tension, could significantly improve the nanotube alignment in the LCs phase[44].

CHAPTER 3

MATERIALS AND METHODS

3.1 General Setup

Semiconducting SWNT (also called IsoNanotubes-STM) and HiPCo SWNT was purchased from NanoIntegris Inc., and used without any further modification. Sodium dodecyl benzene sulfonate (NaDDBs) was purchased from Sigma Aldrich Company. Whatman® Anodisc 47 inorganic filter membrane was purchased from VWR Scientific International. Fisherbrand 75 mm × 50 mm glass slides were used extensively for fabricating the LC-CNT PDMS composites. An 808 nm near infra-red laser of ~160 mW served as the illumination source. All experiments were conducted in a climate-controlled laboratory. Test equipment was operated inside a light-isolated enclosure mounted on an active-air suspension table. Webcams inside the testing enclosure were continuously monitored to ensure all control gear operated properly.

3.2 Actuator Fabrication

SWNT in aqueous solution (1 mg in 100 ml) was prepared by mixing pre-determined volume of nanotube stock solution (~0.1 ml) with known volume of surfactant NaDDBs (~14.9 ml). Then DI water is added (~85 ml) to make the entire contents to 100 ml. The volume of nanotube stock solution and the surfactant is changed to make the five different nanotube solutions with concentrations namely ~0.01 μg/ml,

~0.05 µg/ml, ~0.1 µg/ml, ~0.3 µg/ml, and~ 0.5 µg/ml respectively. Then the contents are ultrasonically agitated for 4 hours. The separated nanotubes well coated with NaDDBS is then filtered using vacuum filtration. Whatman® Anodisc 47 inorganic filter membrane is used as filter for collecting the nanotube LCs films.

PDMS silicone elastomer obtained from Dow Corning (Sylgard 184) was used as the host matrix. PDMS is a two-part solvent-free flexible silicone organic polymer in the form of a base compound with a separate hydrosilane curing agent that acts as a crosslinker. A crosslinker was added at a ratio of 1:10 and mixed for 5 min. To remove trapped air pockets, the prepared polymers were degassed for 30 min.

Figure 3.1 presents the schematic of the single wall nanotube (SWNTs) LCs and the resulting photomechanical composite actuator. Vacuum filtration was used to make the nanotube LC films. The nanotube-surfactant solution, when filtered through the membrane, creates a concentration gradient due to change in fluid velocity across the membrane[10]. As the solution is filtered off and the concentration of nanotube increased, nematic domains form. As presented in Figure 3.1 schematic, nanotube LCs are formed on a Whatman® Anodisc 47 inorganic filter membrane. The LCs from the membrane are then subsequently transferred to a PDMS surface that is spin coated on a glass slide. The membrane is then gently peeled off the PDMS surface leaving the oriented nanotubes on the surface. A second PDMS layer is then spin coated and polymerized to preserve the internal orientation of the film. This work removes impediments in nanotube dispersion and fabrication process such as shear mixing[13], evaporative cross-linking[51, 52], functionalization in acids[53], all of which are challenging and can affect the overall mechanical properties of the composites. Further,

the lack of standards in preparing CNT based composites to date makes them prohibitively expensive and hampers commercialization[54].

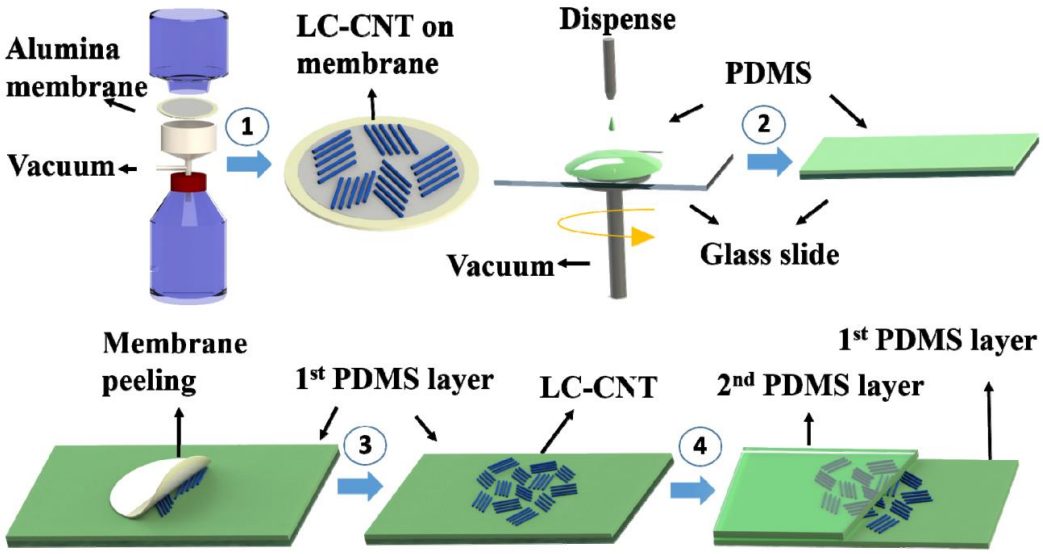

Figure 3.1 | Nanotube Liquid Crystal Elastomer Composite: 1. Vacuum filtration is used to deposit carbon nanotubes (SWNTs) onto an inorganic filter membrane. **2**. PDMS is spin coated on top of a glass slide **3.** The membrane consisting of LCs is pressed against the PDMS that resulted in complete transfer **4.** A second PDMS layer is spin coated and polymerized to enable LC being part of the polymeric network resulting in "Nanotube LC Elastomer".

3.3 Photomechanical Stress Test

PDMS composite test samples were mounted vertically between two clamps as shown in Figure 3.2. The bottom clamp was attached to a weighted (~68.6 g) base and placed on a high accuracy balance (Acculab ALC-80.4). The upper clamp was attached to

an automated linear actuator that was in turn mounted to a high accuracy manual positioning stage. The laser diode was placed ~75 mm from the middle of the test strip such that illumination impacted normal to the PDMS surface. Deformation in the composite strips as a result of NIR illumination caused a change in weight readings on the balance. Once the light was turned off, both the actuator and balance returned to their original length/reading, respectively. Actuation was quite repeatable from cycle to cycle with nearly the same displacement amplitude. Stress test standardization was accomplished by finding the zero strain value of each sample and zeroing the balance. Stress test on each sample was conducted with pre-strain values ranging from 3% to 50%. The timing sequence for each pre-strain value was 1-minute relaxation wait followed by 5 cycles of NIR illumination on for 60 seconds, and then off for 30 seconds. Engineering stress calculations (referred to as stress throughout the paper) were made by dividing the change in force between illumination on and off by the cross-sectional area of the test samples.

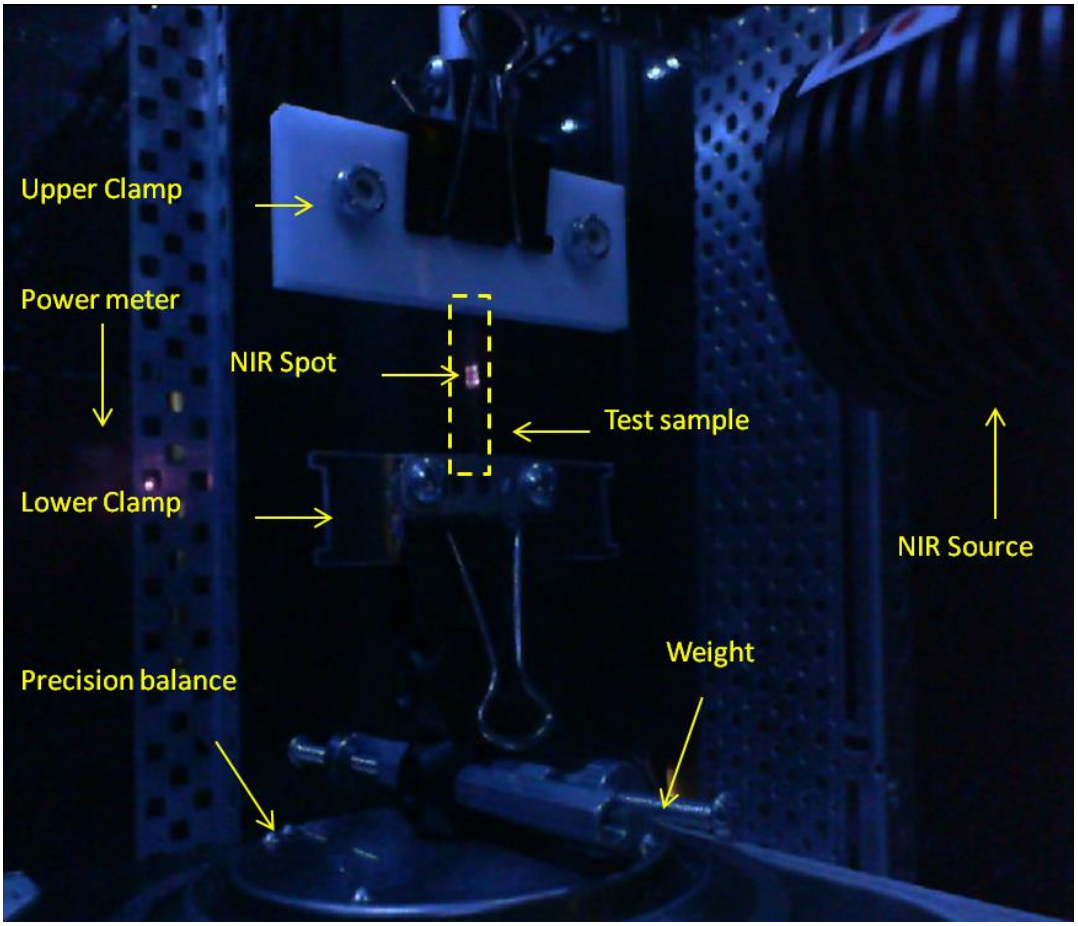

Figure 3.2 | Video Capture of Test Sample and Dynamometer: Test set up enclosed inside a black box to avoid stray light from affecting the measurements. Test sample between the clamps mounted on a precision balance, NIR source used for excitation and manual positioner with linear actuator to apply pre-strains.

3.4 Polarized Optical Microscopy

Olympus IX-71 Inverted Research Microscope with PixeLink Camera (3.0 MP) was used for the polarized image analysis. All the specimens were brought to focus in the brightfield (BF) observation (with no optical element engaged in the light path). IX2-AN polarizer was then employed for polarized light observation. Rotational polarization was done by rotating the polarizer knob t horizontally to get a different angle polarized light (0°and 5°). The characteristic of the domain size and the domain count were measured using image analysis software Image J from NIH.

3.5 Stress-Strain Test

Stress versus strain tests were conducted by Rheometric System Analyzer (RSA-3, TA instruments-Waters LLC) at the room temperature. Multiple extension mode was selected and four zones of separate extension test were performed. The zone time was set at 20 s, 10 s, 30 s and 20 s while the extension rate was set at 0.05 mm/s, 0 mm/s, 0 mm/s and 0.05 mm/s separately, typical for viscoelastic polymers. Stress and strain curve was then plot by Igor and the linear curve fitting was performed to calculate the elastic modulus (E).

3.6 Scanning Electron Microscopy

SEM was conducted using a Zeiss SUPRA 35VP field emission scanning electron microscope. All the specimens were observed under InLens Detector (WD 3mm optimal) with 10.0 kV accelerating voltage.

3.7 Raman Spectroscopy

Raman spectrum of carbon nanotubes, PDMS and their composites were conducted using an inVia Renishaw Raman spectrometer. The ~632.8 nm line beam of a helium-neon laser was focused onto the sample surface through a ×50 objective lens, forming a laser spot approximately 3 μm in diameter. Raman measurements were conducted in at least five different locations in each sample for statistically confident values. A Lorentzian profile was used to fit the Raman peaks in Igor software. The D band, 2D band and G band of the Raman peaks in nanotube LC were identified. All the 9 peaks of PDMS that correspond to polymer chain rotation, translation and stretching were identified.

3.8 X-ray Photoelectron Spectroscopy

MultiLab 3000 VG Thermo Scientific surface analysis system was used for the x-ray photoelectron spectroscopy (XPS) measurements. Mg Kα (1253.6 eV) radiation was used as the excitation source. Binding energy range for survey scanning is from 0 to 700 eV and PASS energy was set as 50 eV. Room temperature and ultra-high vacuum (UHV) conditions at pressures in the 10^{-9} Torr range were maintained during the measurements. Charging of the samples was calibrated by setting the binding energy of the adventitious

carbon (C1s) at ~284.6 eV. Atomic Sensitivity Factors (ASF) was included during bond ratio calculation and C1s was set for ~0.205 and O1s was set at~ 0.63. A Gaussian profile was used to fit the XPS peaks with XPSPEAK software.

3.9 Optical Characterization of Order Parameters Using Dichroism

Carbon nanotube film was transferred to a glass substrate. The film was imaged by SEM and optical polarization microscopy. The sample was illuminated with a white light source. The objective used was 60x, 0.90 NA. Beyond the output polarizer, a 200mm focal length lens projected the image directly onto a CMOS camera sensor (Pixelink PL-B776F) mounted 1.2 m from the lens.

The polarizer and analyzer were both rotated to the vertical direction of the camera sensor. The parallel configuration of the polarizers was verified by rotating the analyzer to maximize the mean intensity recorded at the camera sensor. Images were recorded of the sample (I), empty glass substrate (I_0), and with the light source obstructed (I_{dark}). Polarizer

$$A = \log\left(\frac{I_o - I_{dark}}{I - I_{dark}}\right)$$

and analyzer were both rotated 90° and the same measurements were repeated. Absorbance is then calculated using the formula below for || and ⊥ configurations.

The Dichroic Ratio is then calculated from absorbance using

$$\Delta = \frac{A||}{A\perp}$$

Finally, the optical order parameter can be evaluated using

$$S_{opt} = \frac{\Delta - 1}{2 + \Delta}$$

3.10 Optical-to-mechanical Energy Conversion Factor and Conversion Efficiency

$$P_{absorbed} = P_{uninterrupted} - P_{sample}$$

$$W_{actuation} = [\Delta\sigma \times A_{cross\text{-}section}] \times d$$

$$E_{absorbed} = P_{absorbed} \times t$$

$$\textit{Opto-mechanical Factor } \eta_M = \Delta\sigma_{total} / P_{absorbed}$$

$$\textit{Energy Conversion Efficiency } \eta = W_{actuation}/E_{absorbed}$$

Newport 1918-C power-meter was employed to measure the power absorbed in the sample. Initially the uninterrupted laser power $P_{uninterrupted}$ was measured. Next, LCs-CNT composite test sample was mounted in front of the power meter and a value of P_{sample} was measured. The difference between $P_{uninterrupted}$ and P_{sample} gives the actual power absorbed by the sample. The optical-to-mechanical energy conversion factor (η_M) is calculated by dividing the total change in engineering stress ($\Delta\sigma_{total}$) from maximum expansion to maximum contraction by the $P_{absorbed}$. Furthermore, $W_{actuation}$ is the work done was calculated by photomechanical stress σ multiplied by $A_{cross\text{-}section}$ and deformation d. The total absorbed energy $E_{absorbed}$ was obtained by the $P_{absorbed}$ multiplied by time t (in this experiment 60 s) Finally the energy conversion efficiency with different concentration and pre-strain is calculated by dividing $W_{actuation}$ by $E_{absorbed}$, resulting in a maximum value of ~0.0045% (~0.5 μg/ml at ~ 50% pre-strains).

CHAPTER 4

RESULTS AND DISCUSSION

4.1 Actuator Fabrication and Characterization

In general, it is well known that shear mixing and dispersion of nanotubes in polymers is difficult process plagued by irreproducibility, lack of electrical conductivity at low concentrations, introduction of defects and even breaking of nanotubes during the shear mixing process, all of which can affect the overall mechanical properties of the composites. We developed a novel protocol to deposit liquid crystal SWNT film on membrane and readily to transfer to polymer surface and preserve the LC structure.

Figure 4.1 presents the photographic images of the samples. Figure 4.1 (a) presents the LCs on the alumina membrane. The numbers 0-5 represent plain alumina membrane and nanotubes at concentrations of ~0.01 μg/ml, ~0.03 μg/ml, ~0.05 μg/ml, ~0.1 μg/ml, ~0.3 μg/ml and ~0.5 μg/ml respectively. The concentrations mentioned above are the starting solution concentrations to make the film using vacuum filtration process. Figure 4.1(b) presents the film after full transfer from membrane to PDMS. Cut photomechanical actuators are presented in Figure 4.1(c).

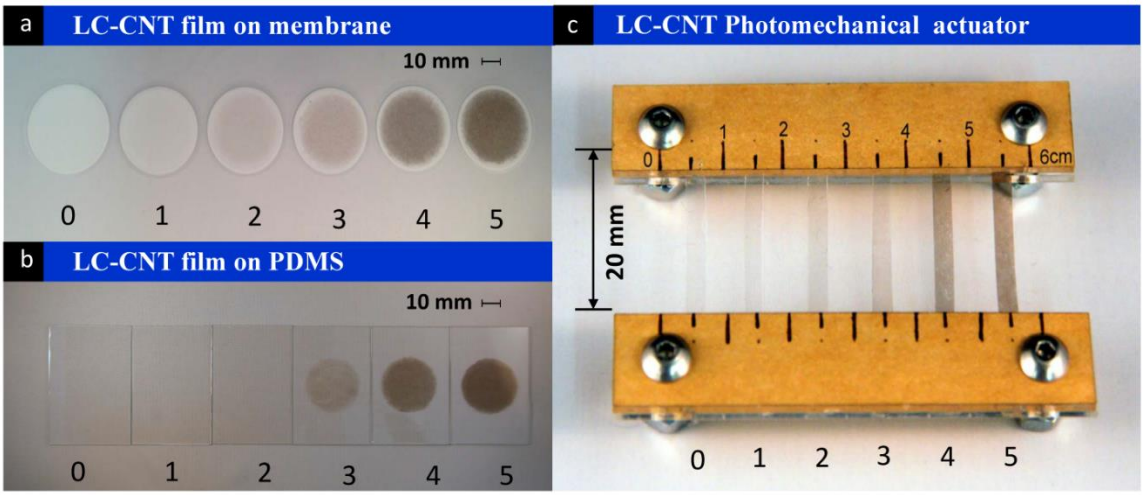

Figure 4.1 | Film Transfer, Actuators: (a) Single wall nanotube (SWNT) liquid crystal films on membrane after vacuum filtration; (b) Fully transferred film onto PDMS; (c) SWNT LC photomechanical actuators. The numbers represents concentrations of CNTs as follows: **0**-plain PDMS; **1**-0.01 µg/ml; **2**-0.05 µg/ml; **3**-0.1 µg/ml; **4**-0.3 µg/ml; **5**-0.5 µg/ml.

It is easily to observe the color of the actuators change to dark gradually from left to right in Figure 4.1. This change is due to different thickness of the SWNT films. SEM was employed to measure the thickness of different SWNT films by scanning the cross-section. Figure 4.2 presents the cross-sectional SEM images of the composites. The actual thicknesses of the films were between ~126-865 nm for the different concentrations mentioned. The thickness of the LC layer increased with concentration. At these measured thicknesses, the starting concentration needed to make a single layer LCs films is anywhere between 58-79 pg/ml. Such ultra-small concentrations with the ability to create ordered films could be highly useful in scalable manufacturing of LCs nanotubes for high performance commercial applications.

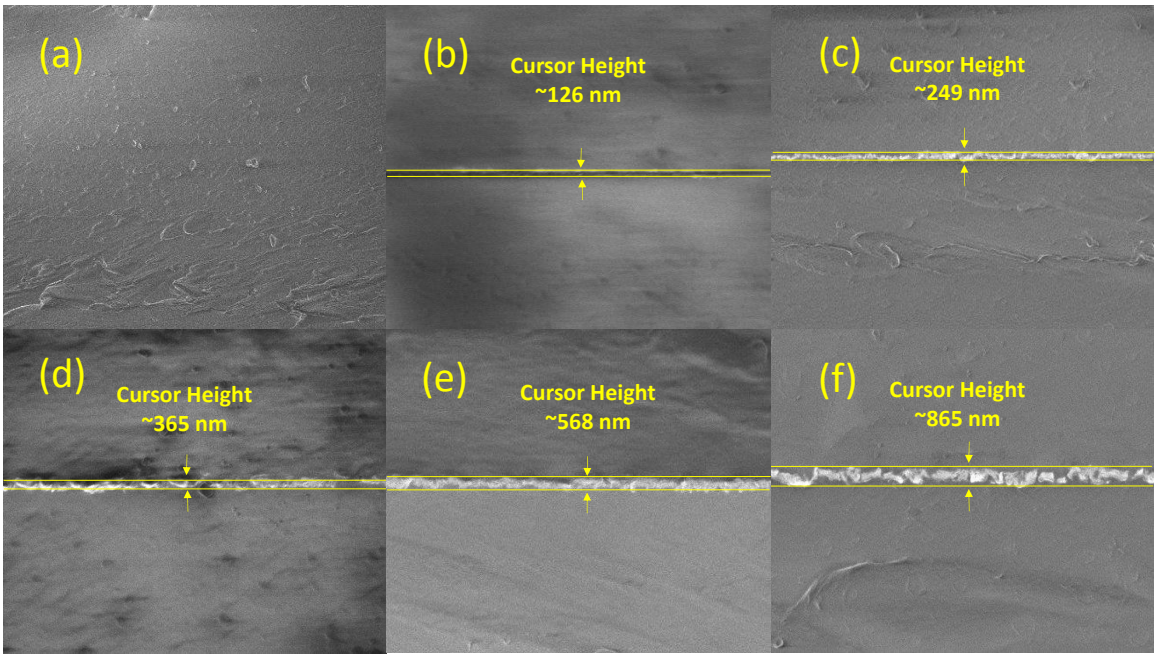

Figure 4.2 | SEM Images of LC-CNTs: Cross-sectional SEM images of nanotube LCs in PDMS matrix for the different concentrations: (a) Plain PDMS; (b) 0.01 μg/ml; (c) 0.03 μg/ml; (d) 0.1 μg/ml; (e) 0.3 μg/ml; (f) 0.5 μg/ml.

Figure 4.3 presents the characterization of SWNT using Raman spectroscopy and X-ray photoelectron spectroscopy. Figure 4.3 (a) presents the Raman spectrum of plain PDMS and LC-CNT/PDMS. A small D band (~1320 cm^{-1}), a large G band (G^{+}~1590 cm^{-1}) and prominent 2D band (2632 cm^{-1}) is clearly seen in the Raman spectrum. The small D band suggests low defect densities in the LC-nanotubes. The G band at ~1590 cm^{-1} is the G^{+} feature which is the in plane vibration of sp^2 bonds along the tube axis. The other peak see in the G band is the G^{-} feature which is around 1570 cm^{-1} is the in-plane vibration along the circumferential direction. Both these features are indicative of semiconducting nanotube-LC. The relative intensity of D to G provides a good indicator for determining the in-plane crystallite size or the amount of disorder in the sample. The

intensity of D to G was calculated from Raman spectrum as I_D/I_G ~0.18. This suggest low disorder and in plane lattice vibration of sp^2 carbon bonds. The intensity of G' band or 2D band is almost twice the D band as is expected for the double phonon process. The I_{2D}/I_G is ~0.46. All these data suggest low defect densities and high quality nanotube liquid crystals. This is also evident in the SEM images in the form of gentle curvature of the nanotubes as opposed to twisting morphologies and shorter nanotube segments around the liquid crystal core which may induce defects in nanotube-LCs.

Figure 4.3 (b) is the X-ray photoelectron spectroscopy of the nanotube LCs. The XPS C1s spectra shows the different binding energy values for different carbon bonds, namely sp^3 C-C or C-H (285.5 eV), single C-O bonds (286.1 eV), and sp^2 C = C bonds (284.6 eV). Figure 3(b) shows the high levels of deoxygenated sp^2 carbon bonds that exist in nanotube LC which was also confirmed by the G bands of Raman spectrum. This also signals high intrinsic thermal conduction along the tube axis which is well-suited for photo-mechanical actuators presented here. The intensity of sp^2 C = C (~46.7%) is much higher than the *sp3* C-C bonds (~17.5%), C-O bonds (~6.6%) and C=O (1.6%). The XPS O1s spectra shows the different binding energy of oxygen single (-O-) bond at ~531 eV and oxygen double bonds (=O) at 533 eV.

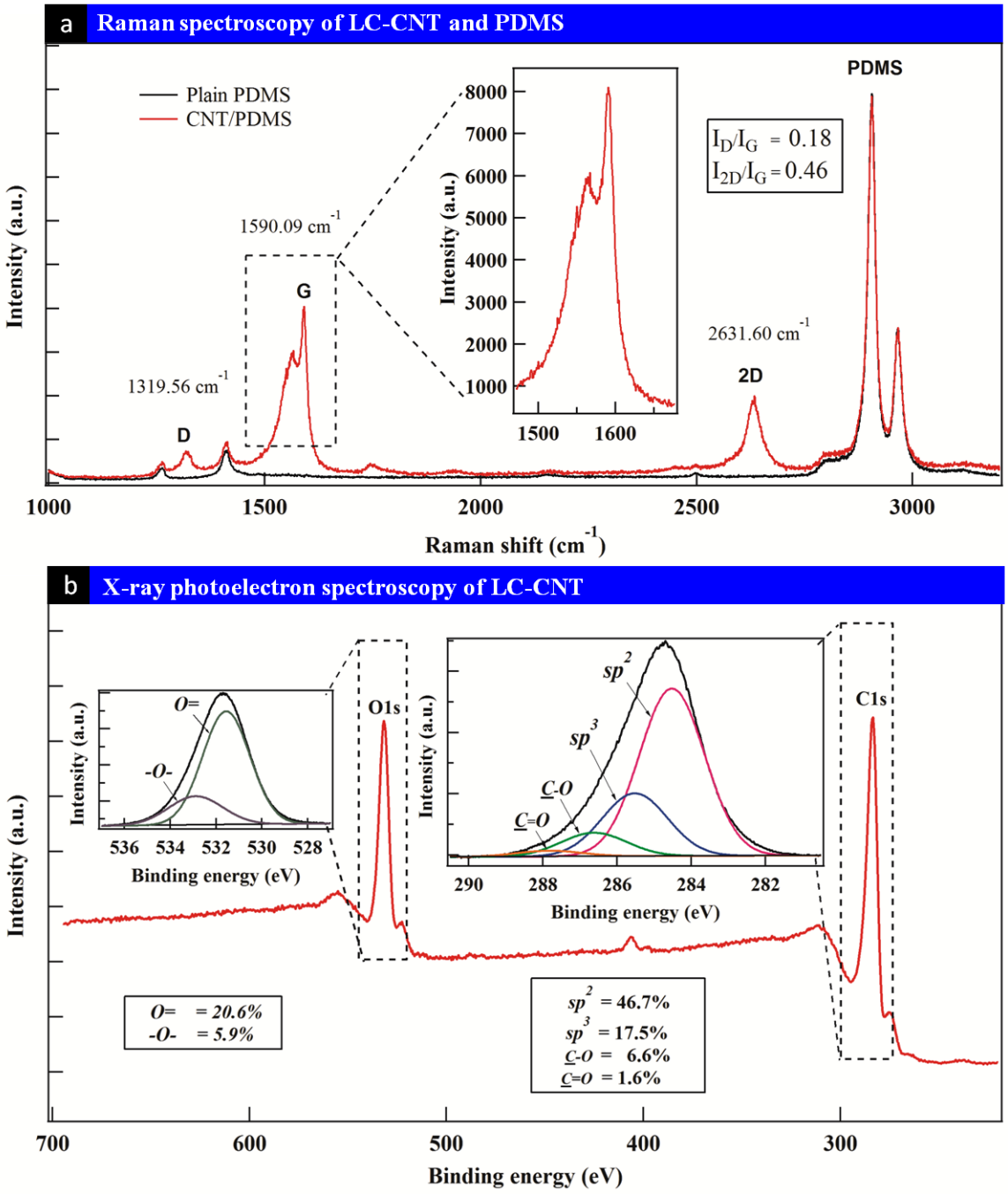

Figure 4.3 | Characterization of SWNT: (a) Raman spectroscopy of CNT and PDMS. A small D band and pronounced 2D and G band is observable. I_D/I_G ~0.18 and I_{2D}/I_G ~0.46 suggest low defect densities and high quality nanotube-LC; (b) X-ray

photoelectron spectroscopy of CNT suggest higher percentage of sp^2 bonds followed by sp^3 bonds.

4.2 Liquid Crystal Structure and Order Parameter

In order to observe the liquid crystal structure of SWNT, SEM was taken again to scan the surface of LCs nanotubes film. Figure 4.4 presents the SEM images of the nanotube LCs nanotubes films. Five columns of images show the evolution of the microstructure at different concentrations. The rows represent the same concentration at different length scales. It is observed that at low magnification (Figure.4.4 (a-1), the lowest concentration film (~0.01 μg/ml) consisted of sets of nucleated nematic islands that were loosely connected by few isotropic nanotubes in between. This is a characteristic two phase behavior of a lyotropic nematic LCs[1]. The minimum concentration required for formation of nematically ordered LC domains was ~0.0075 μg/ml. Below this concentration, the films were purely isotropic[10]. As the concentration of the nanotube in solution increased, nucleated nematic regions grow as seen with the increase number of island in Figure 4.4 (b-1, c-1). In Figure 4.4 (d-1), the nucleated nematic islands become larger domains thereby closing the gap between adjacent islands. Finally in Figure 4.4 (e-1), the films are continuous and bridge all the gaps forming large nematic domains as in refining its own structure/self-healing to achieve final film morphology. Row 2 and Row 3 are the images at 1 μm and 200 nm scale respectively. In Row 2, the nematic like LC texture of film is clearly observed with nanotubes oriented along a specific nematic director. It is evident that ± ½ disinclinations are formed, as in[9], confirming the topology of the nematic phase. In Row 3, the morphology of all the films looks similar after the isotropic-

nematic transition. For clarity one of the images is enlarged (Figure 4.4 (f)) to show the ordered arrangement of nanotubes.

The insert image Figure 4.4 (g) shows the concentration dependence of the local order parameters above the isotropic-nematic transition. There are pores in between the bundles across all the concentrations and there is a twisting pattern of individual nanotubes due to rotation of the nanotube. The competing scenario between translational and rotational entropy of nanotubes thus determines LCs texture and order parameters. It is also seen that the orientation of the nanotubes during vacuum filtration occurs in bundles and not individual tubes due to the inter-tube attraction between the nanotubes. These bundles are 10-20 nm in diameter. In Row 3, it is observed that irrespective of the concentration at nanometer length scales most films have similar orientation in their nematic domains with slight changes in the order parameters.

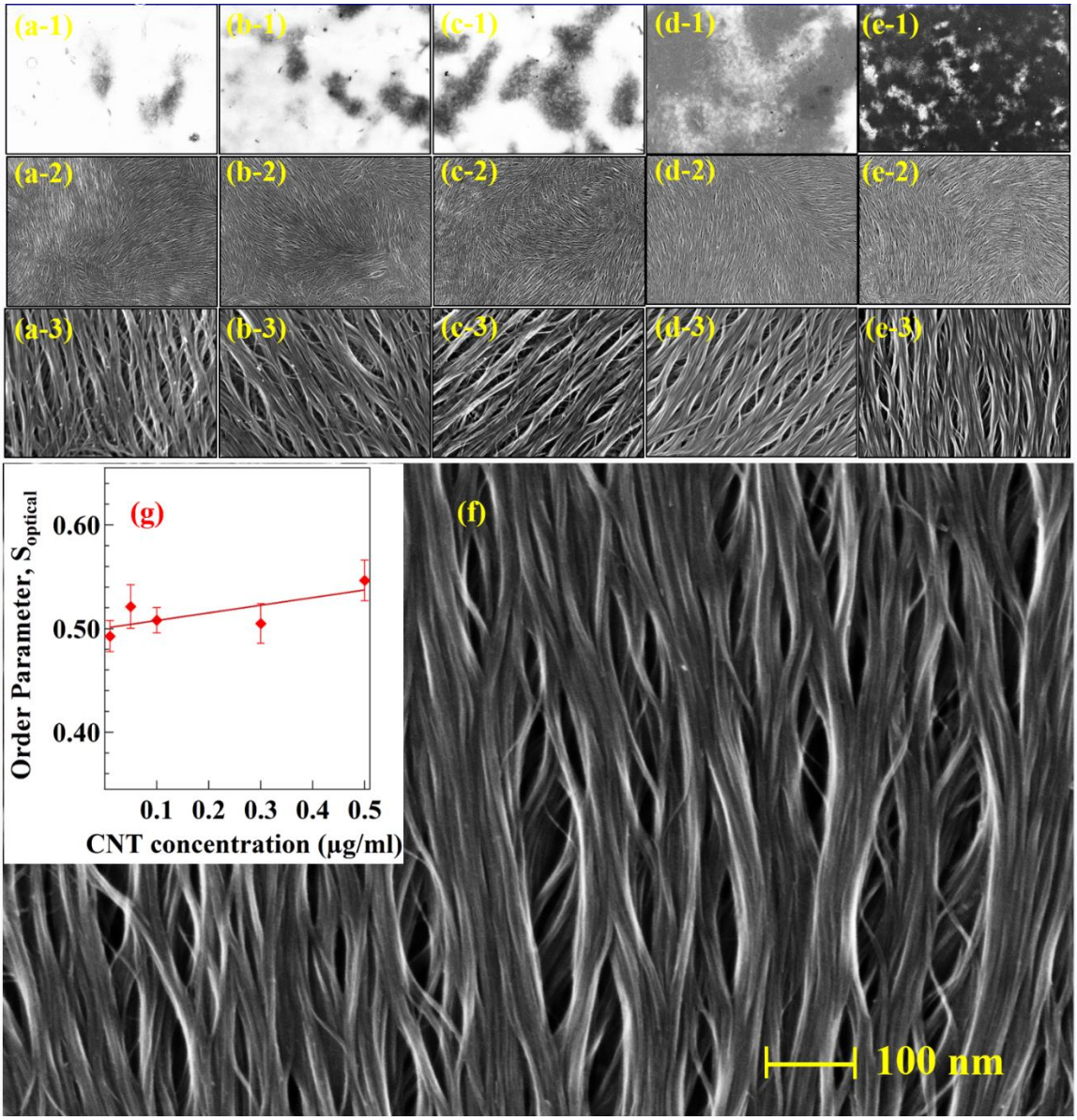

Figure 4.4 | SEM Images of LC-CNTs Surface: (a-1)- (a-3)): 0.01 μg/ml; (b-1)- (b-3)): 0.05 μg/ml; (c-1)- (c-3)): 0.1 μg/ml; (d-1)- (d-3)): 0.3 μg/ml; (e-1)- (e-3)): 0.5 μg/ml; Scale bars: Row 1: (a-1)-(e-1): 10 μm; Row 2: (a-2)-(e-2): 1 μm; Row 3: (a-3)-(e-3): 200 nm, (g) order parameter versus concentration and (f) magnified image of (e-3)

Figure 4.5 presents the bright field image (top row), the image under cross-polarizers (middle row) and polarized image with 5 degree rotation of the polarizers

(bottom row). The columns (a-f) represent different concentrations of the nanotube in the composites. Yellow arrows indicate the bright regions turning dark and vice versa for polarized image and the rotation of the polarizer by 5 degrees. The bright and dark regions represent the domains where all the nanotubes are oriented in one specific director. The high intensity of the bright spots in the polarized image suggests strong birefringence of the domains. The light and dark areas represent different orientation, birefringence and length. Since these are not constants one can see differing regions across the spectrum of concentrations. Further, zooming in the high concentrations, one can also see some of the domains are green in color. The number of green domains increases with concentration. The color of these domains may be indicative of optical filtering due to the spacing between the nanotube bundles in those domains, their length and orientation. Color patterns similar to the one observed here in the polarizing microscope are very useful in the study of nanotube liquid crystals, including the identification of textures, of liquid crystal phases (isotropic versus nematic) and the observations of phase changes. Such color patterns could also be useful in studying strains where the change in strain can shift the wavelength seen through the polarizer and its color.

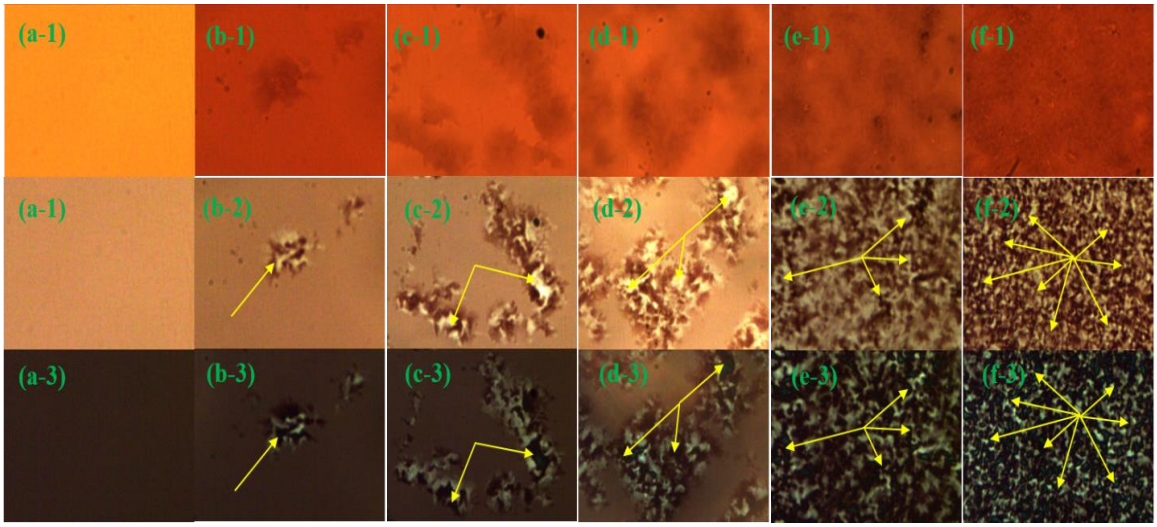

Figure 4.5 | Birefringence of Liquid Crystal Nanotube Polymer Composites: Each column represents a concentration of nanotube liquid crystals in PDMS starting with plain PDMS (a-1 to a-3); 0.01 µg/ml (b-1 to b-3); 0.05 µg/ml (c-1 to c-3); 0.1 µg/ml (d-1 to d-3); 0.3 µg/ml (e-1 to e-3) and 0.5 µg/ml (f-1 to f-3). The top row is bright field image; middle row is the polarized image under cross polarizers; and bottom row is the image under cross-polarizers with 5 degree rotation of the polarizer.

Any LCs anisotropy is defined by its order parameter. In two dimensions, the order parameter is given by:

$$S = \quad < 2\cos^2\theta - 1 >$$

where the brackets denote the average over the ensemble of all angles. *S* is therefore at a maximum of 1 when all CNT are aligned in the direction of θ, and a minimum of -1 when all CNT are perpendicular to θ. Order parameter was calculated for individual domains from the SEM images with the aid of 2D Fourier analysis similar to one used by Bayan, *et al* for collagen fiber orientation . These yielded values of S=0.77-0.88 for the different LCs

films. These were also compared to the randomly oriented films which yielded average order parameters of S=0.06-0.24 (~4-13 times smaller) for the same concentration.

While the order parameter is easy to calculate from SEM images using the 2D FFT analysis, it is important to validate this method through measuring order parameters using polarization optical microscopy[55]. The order parameter of the nanotube LCs was ascertained using polarization microscopy[55]. Films were transferred to a glass sample and the order parameter of the films was calculated using both FFT analysis and polarization microscopy. The order parameter using polarized microscopy was evaluated by using dichroic ratio Δ given as the ratio of absorbance that is parallel and perpendicular to the director.

Figure 4.6 presents the linear correlation between the order parameters from both the methods. The order parameters measured using polarization microscopy was smaller than the 2D FFT by factor of ~1.5. A linear relation between order parameters from both techniques was established:

$$S_{FFT} = 1.49 \times S_{optical} + 0.01$$

The FFT technique although produced a higher order parameter is easier to quantify based on SEM images of the nanotube liquid crystals without additional experiments. The relationship is useful in calculating any future order parameters of nanotube films for their alignment and one can get a realistic estimate of order parameter without resorting to transferring films onto glass slides and additional polarization microscopy experiments. All the data reported from hereon has the corrected order parameter based on the optical measurements. Thus the order parameter mentioned above using FFT for LC films can be corrected to $S_{optical}$=0.51-0.58 and for randomly oriented film $S_{optical}$=0.04-0.16.

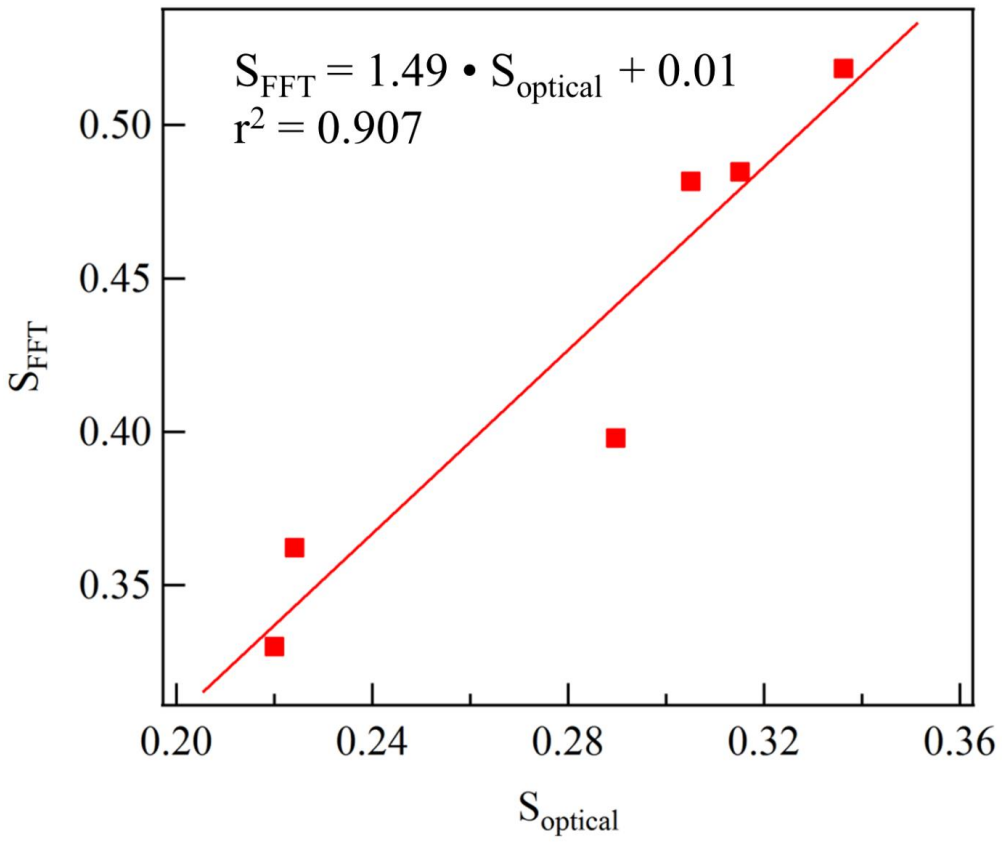

Figure 4.6 | Order Parameter: Linear correlation between spatial frequency and optical order parameter

Figure 4.7 (a) presents the *Schlieren textures* of nanotube LC films suggesting nematic orientational order in the macroscopic composite. At 2.5 degree rotation of the polarizer, due to enhanced contrast, the domain walls are visible with each domain aligned along a specific director. Measuring domain size as a function of concentration yielded dramatic results which are presented in Figure 4.7 (b-g). The domain counts and size were calculated based on the particle analysis function in NIH Image J software for the polymer composites from the binary images[56]. The size of these domains were anywhere from 1 μm^2 to 150 μm^2. It is seen that with increase in concentration, the domain size decrease significantly. The number of domains per mm^2 (~5-10 μm^2 size) is seen to increase from

260 domains/mm^2 at ~0.01 μg/ml to 14,367 domains/mm^2 at ~0.5 μg/ml. As the concentration increases, the film also spreads over a large area however making the domain size smaller suggesting large number of directors for formation of LCs in subsequent layers. As the nanotubes arrange in different layers, some of these nanotubes spontaneously become directors for the formation of individual domain thereby making the process more localized resulting in smaller domains as the film spreads over large area.

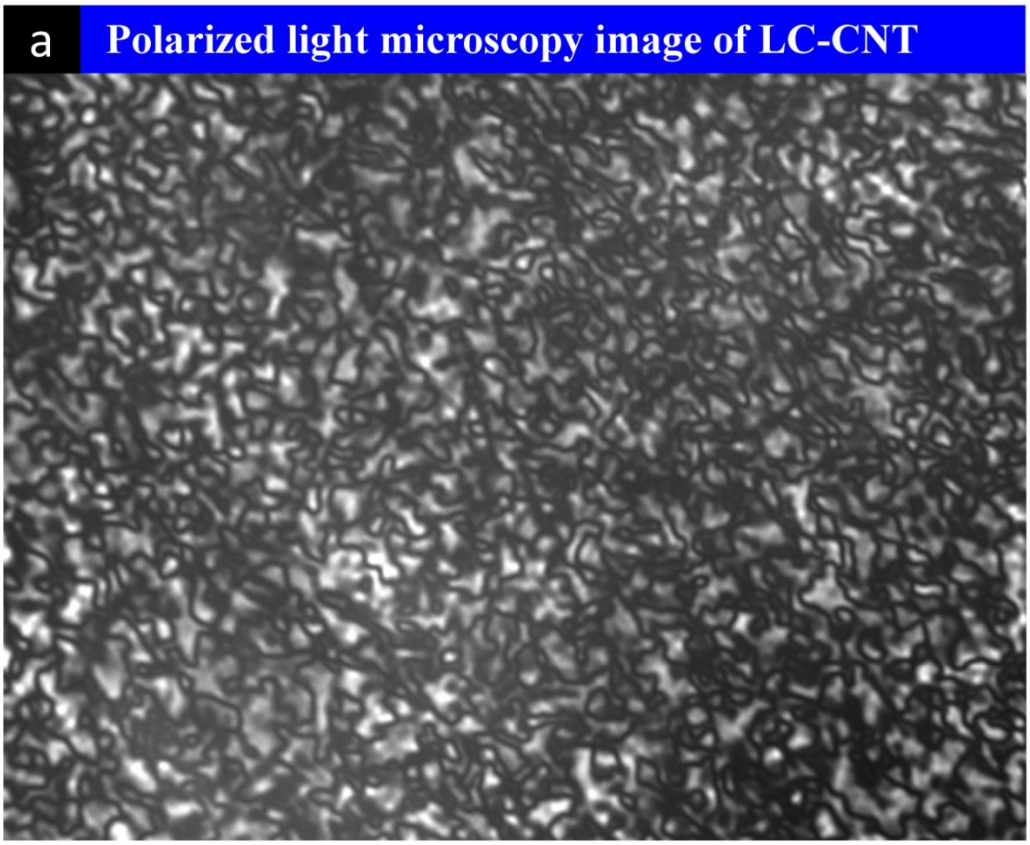

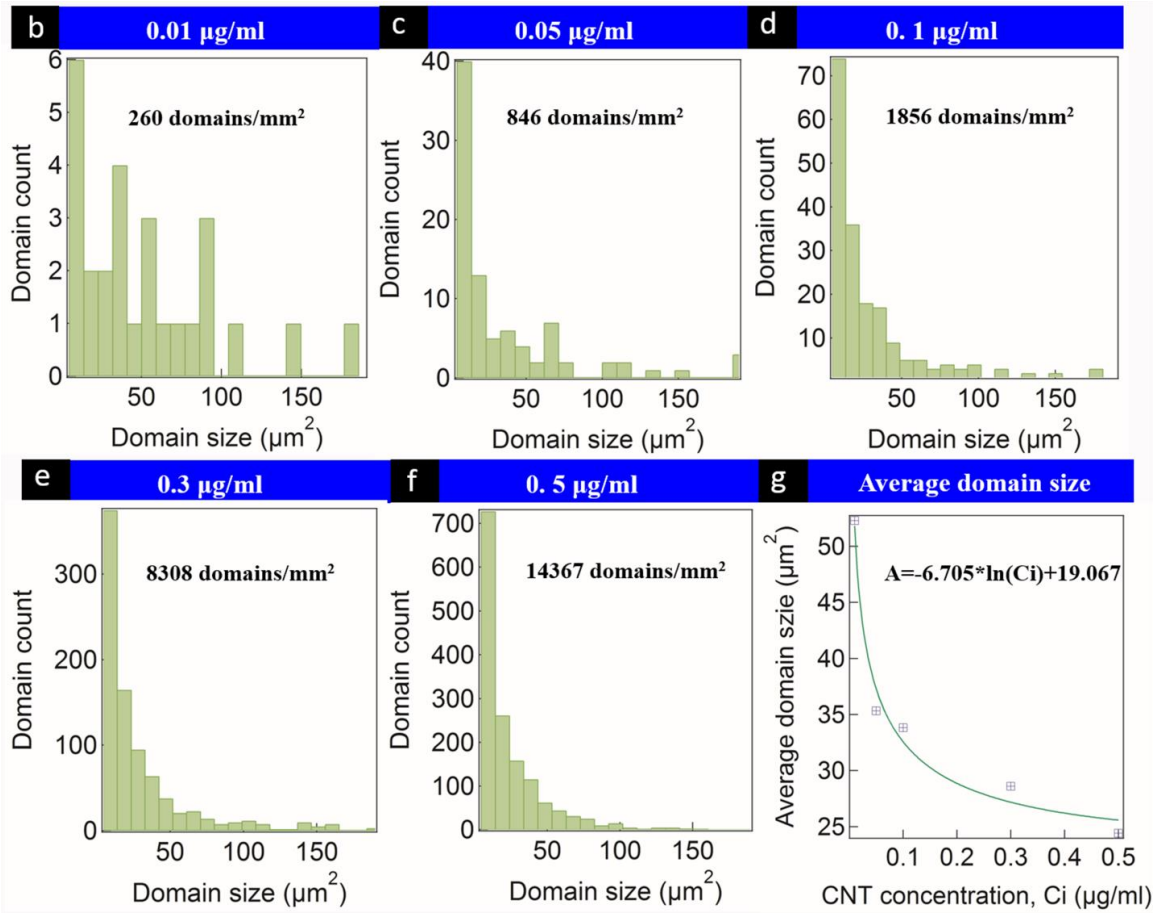

Figure 4.7 | Schlieren Textures and Domain Size Analysis: (a) Schlieren textures of nanotube LCs: Rotation of the polarizer by 2.5 degrees (92.5 degrees) resulted in enhanced contrast and better imaging of the *Schlerien* textures and domain walls suggesting long range order. Scale bar: 2 mm. (b-g) Domain Size Measurements as a function of concentration inside the LC-polymer composites: (b) ~0.01 µg/ml; (c) 0.05 µg/ml; (d) ~0.1 µg/ml; (e) 0.3 µg/ml; (f) ~0.5 µg/ml; (g) Average domain size versus CNT concentration showing almost twice the decrease in domain size with increasing concentration. Line is shown for eye guidance only.

4.3 Mechanical Property, Photomechanical Response and Energy Conversion

Figure 4.8 presents the elastic modulus versus weight fraction of nanotubes in polymer composites. The elastic modulus is seen to increase with concentration of nanotubes at these ultra-small concentrations (<1.4 x 10^{-2} wt.%). At low mass fractions (~0.5 x 10^{-2} wt.%), the elastic modulus of the composite is seen to be only dependent on the nanotube fillers. Insert presents the change in elastic modulus of such ordered LCs composites. The change in elastic modulus E ~20-95% was seen for the concentrations used which had high order parameters between $S_{optical}$=0.5-0.6 (above the isotropic-nematic transition). It should also be noted that the ~20% change in E was achieved for just ~3 x 10^{-3} wt.% of nanotube and >90% change in elastic modulus of composite was achieved for mere <1.4 x 10^{-2} wt.% of nanotube, about 100 times smaller weight fractions than past reports[57]. The use of surfactant enabled nanotube LCs thus presents a more environmentally benign approach (no acid treatment or functionalization), easier sample preparation, order dependent elastic modulus for low mass fraction of nanotubes to prepare composites.

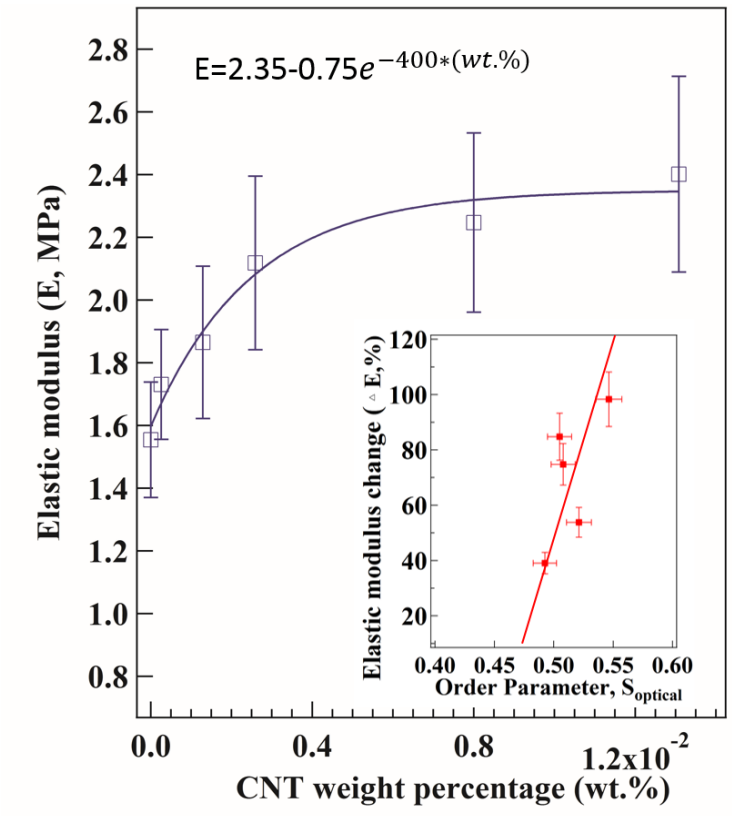

Figure 4.8 | Elastic Modulus vs CNT Mass Fraction in Composite: Insert is the change in E with order parameter in polymer composite.

Photomechanical responses of nanotube LC-polymer composites are presented in Figure 4.9(a-f). Starting with a plain PDMS elastomer (figure 4.9 (a)) and progressing from ~0.01 µg/ml to ~0.5 µg/ml concentrations of nanotube-LCs/PDMS composites (figure 4.9 (f)), each plot shows the photomechanical response to ~808 nm NIR illumination for five consecutive cycles each one being 60 s. Since the optical loss of PDMS in the NIR region is <0.5 dB cm−1[58], the negligible/zero response in the plain PDMS sample (figure 4.9 (a)) was expected. However, by a concentration of ~0.01 µg/ml (figure4.9 (b)), the photomechanical effect becomes clearly observable through expansion and contraction of the actuator. Inset in Figure 4.9 (b) clearly shows the

expansion for low pre-strains and contraction for moderate to high pre-strains. All the composites exhibited that low pre-strain values resulted in positive film expansion and thus positive-induced stress, while high pre-strain values resulted in contraction (negative thermal expansion) and thus negative change in stress. More concisely stated, weakly stretched composites show reversible expansion while highly stretched composites show reversible contraction suggesting rubbery elasticity. At ~9 % pre-strain, the samples exhibited zero stress or no photomechanical actuation. This cross-over from small positive expansion to large negative expansion suggests rubbery elasticity at the thermo-elastic inversion point[12]. The magnitude of the photomechanical response was negligible (no movement) for plain PDMS, +0.10 kPa to -0.25 kPa for ~0.01 μg/ml, +0.7 kPa to -2.2 kPa for ~0.05 μg/ml, +2.8 kPa to -7.2 kPa for ~0.1 μg/ml, +5.5 kPa to -14.7 kPa for ~0.3 μg/ml and +8.0 kPa to -22.8 kPa for ~0.5 μg/ml concentrations of nanotube LCs. Each plot in Figure 4.9 also shows the entire 5 cycle response and shows reproducibility from one cycle to the next. Such photomechanical actuators have been operated continuously in our laboratory for more than 3000 cycles without degradation[51].

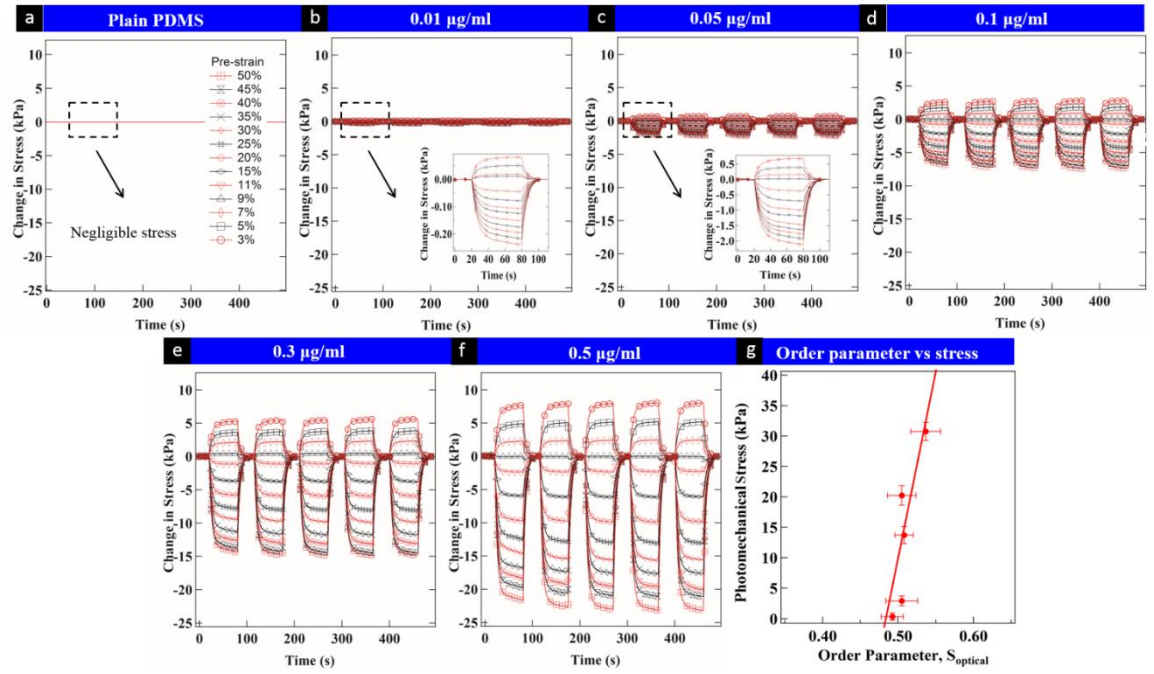

Figure 4.9 | Photomechanical Responses of LCs-CNT Polymer Composites: Pre-strains from 3-50% were applied before NIR excitation: (a): plain PDMS; (b): 0.01 µg/ml; (c) 0.05 µg/ml; (d) 0.1 µg/ml; (e) 0.3 µg/ml; (f) 0.5 µg/ml; (g) photomechanical response versus order parameter demonstrating increased ordering leads to improved mechanical response of the composites.

One interesting question that arises is the effect of nanotube ordering on the photomechanical response. In order to investigate this, films with exact concentrations (~0.5 µg/ml) and same nanotube purity were processed into both randomly oriented bucky papers ($S_{optical}$ =0.16) and surfactant processed liquid crystal films ($S_{optical}$ =0.58). The thickness of the sample was quite similar after vacuum filtration and film transfer. Figure 4.10 (a) and (b) presents the SEM images of the randomly oriented and liquid crystal films respectively. The difference in morphology is easily seen with ordered arrangement of

nanotube in Figure 4.10(b). Subsequent testing for photomechanical response suggested almost 3 times smaller in photomechanical response for randomly oriented sample compared to the liquid crystal sample as presented in Figure 4.10(c-d). This unambiguous result suggest that for same concentration, the photomechanical response, the kinetics and the energy transduction all depend on the order of the nanotube in film. This may suggest that the overall photomechanical response may be sum of individual nanotube-polymer response around the light spot. Using high quality randomly oriented films only resulted in lower response. The result in Figure 4.10 (c) (0.5 μg/ml randomly oriented) can be compared to Figure 4.9(c) (~0.5 μg/ml LC nanotubes), 10 times small amount of mass. The use of randomly oriented films thus leads to higher cost and moderate performance compared to self-assembled liquid crystal films which can access the superior nanotube properties.

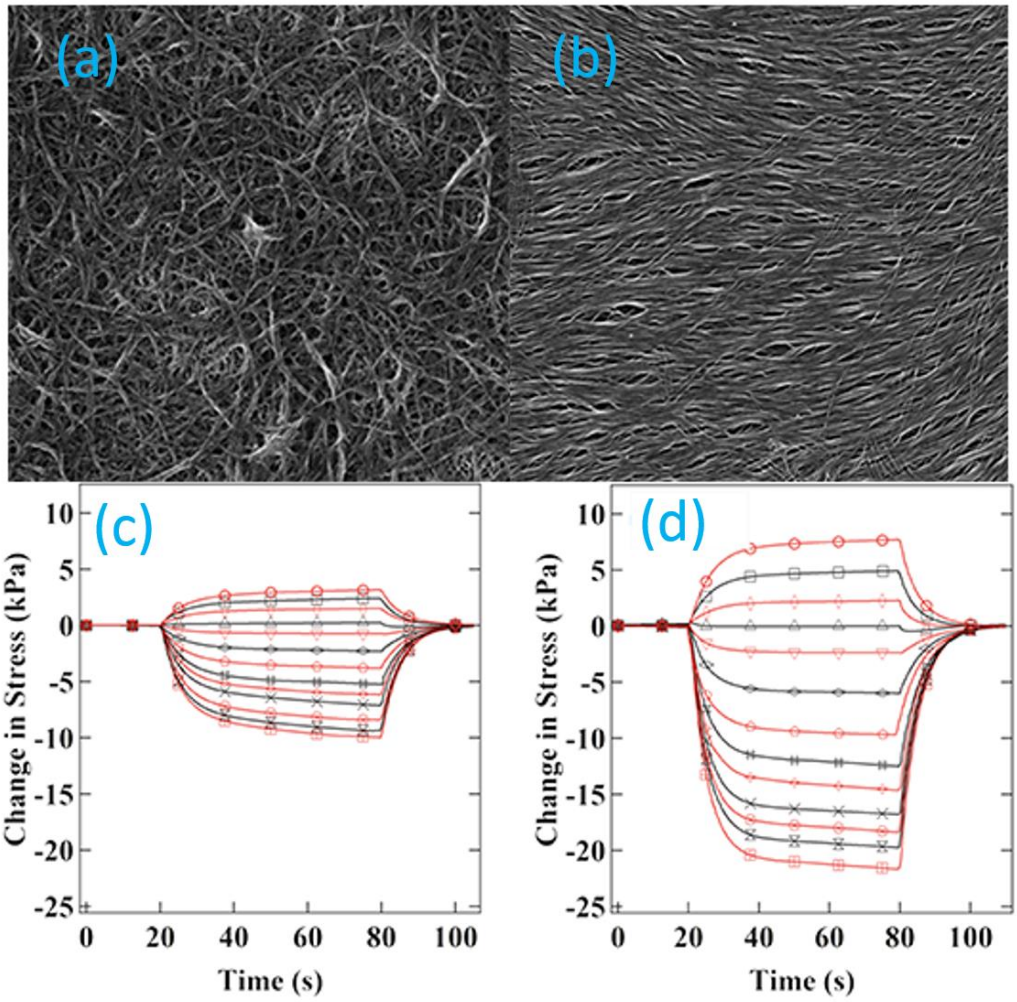

Figure 4.10 | Disordered vs Ordered Systems:(a) SEM image of randomly oriented film (~0.5 μg/ml concentration with order parameter $S_{optical}$=~0.2); (b) SEM image of LCs nanotube film (~0.5 μg/ml concentration with order parameter $S_{optical}$=~0.6); (c) Photomechanical stress change for randomly oriented film based actuator; (d) photomechanical stress change for LCs film based actuator.

Investigating the kinetics of actuation and relaxation, nanotube LCs elastomer composites demonstrated actuation kinetics that was fitted as per the Kohlrausch-Williams-Watts (KWW) function for actuation $\Delta\sigma_{actuate}(t) = 1-exp[-(t/\tau)^{\beta}]$ and relaxation $\Delta\sigma_{relax}(t) = exp[-$

$(t/\tau)^{\beta}$][59]. Figure 4.11 (a) & (b) presents the actuation and relaxation kinetics fitted to the KWW functions for both expansion and contraction respectively. What's interesting is the time constants τ=7 s for actuation and τ=5 s for relaxation is seen with stretching exponent $\beta_{actuation}$ =0.91 and $\beta_{relaxation}$=1.04. The stretched exponential function contains just two free parameters: the relaxation time τ and the fractional "stretching" exponent β, which satisfies $0 < \beta \leq 1$. The upper limit of $\beta = 1$ corresponds to simple exponential decay or Debye relaxation, while lower values of β are indicative of a more complicated non-exponential relaxation process or viscoelasticity[60]. The results here suggest that on NIR excitation, heating the nanotubes and subsequent movement of polymer chains is a highly complex process. While τ is a material sensitive parameter, we investigated how β varies with nanotube concentration and pre-strains to investigate the topographical origin of β. We assumed it would be constant and independent of nanotube concentrations and pre-strains. Figure 4.11 (c) & (d) presents the stretching exponent β as a function of nanotube concentration and pre-strains respectively. Several interesting things can be seen. The stretching exponent β is almost constant (β<1) with increase in nanotube concentration for relaxation. For actuation, β is seen to decrease, reach a minimum (β=0.8 at 0.2 μg/ml) and then goes back up (β=0.9 at 0.5 μg/ml) suggesting both short and long range interactions. With increase in pre-strains, the variation of β is also seen in actuation. This variation of β may be due to change in microscopic order of the nanotubes after stretching resulting in more complex chain movements and longer range of interactions of the disordered polymer when excited by NIR light. However, in both cases of relaxation β almost tries to approach unity at high concentrations and pre-strains. The variation in β also could mean dynamic changes in rheological properties of the sample with light excitation, pre-strains and

nanotube concentrations. We tried to fit the actuation and relaxation with β=2 as in the past which was far worse compared to past nanotube photomechanical actuators[61]. Therefore this study shows that design of photomechanical actuators whether layered composite or nanocomposite encompassing the same material can have two different responses and therefore is a highly complex but interesting system to study.

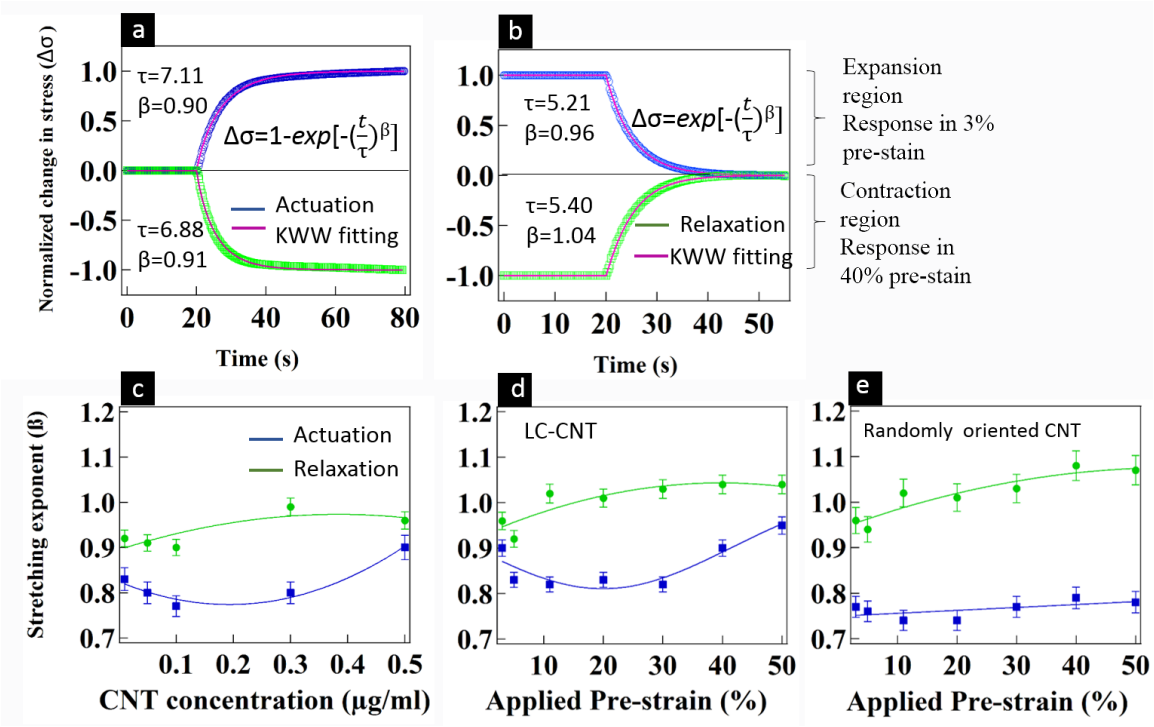

Figure 4.11 | Kinetics of Photomechanical Actuation in Nanotube LCs elastomer:(a) Actuation kinetics; (b) Relaxation kinetics; (c) Variation of stretching exponent for both actuation and relaxation as a function of concentration of nanotube liquid crystals in elastomer; (d) Variation of stretching exponent with pre-strains for LC-CNT. (e) Variation of stretching exponent with pre-strains for randomly oriented CNT.

Nanotube-LCs addition to elastomers not only creates high mechanical strength composites and photomechanical actuation, but also could potentially be viable system for energy harvesting. We calculated some optical to mechanical conversion factors. Figure 4.12 (a) presents the optical to mechanical conversion factor versus concentration. This number is a measure of stress generated to the power absorbed by the actuator light spot and has been reported in the past as a measure of photomechanical actuator performance[13, 62]. A factor of ~0.5 MPa/W was measured for the nanotube LC elastomeric actuator. These numbers are similar to past carbon nanotube and more recently graphene based photomechanical actuators 0.5-10 MPa/W[12, 13]. However, in contrast to all previous work, the amount of carbon nanotube used in the present work was ~100-1000 times smaller and our design is a layered composite unlike past nanotube/graphene photomechanical actuators which were nanocomposites[12, 13]. Further, the mass fractions used were also ~10,000 times smaller than past electro-mechanical actuators based on nanotube polymer nanocomposites[14]. This may suggest that instead of mixing nanotubes into polymer resulting in nanocomposites, high quality nanotubes at ultra-low concentrations that are self-assembled into LCs with layered design may potentially lower the cost for commercial applications. This may especially be true for thin film transistors where accessing the extraordinary properties of nanotube LCs may result in high electron mobility. We therefore believe the commercialization of nanotube products is thus one of design and understanding the trade-offs between performance and material utilization.

An important aspect of any actuator is the energy efficiency at converting external stimulus into useful work. Therefore, efficiency (η) of the nanotube-LCs composites to a known IR illumination source was evaluated. Figure4.12 (b) presents the efficiency as a

function of nanotube-LC loading. The efficiency increased with increase in concentration which ranged from ~ 0.0015% (0.01 µg/ml at 50% pre-strains) to ~0.0045% (~0.5 µg/ml at ~50% pre-strains), about 3 times increase at such small nanotube-LC concentration. Further, efficiencies were also observed to be tunable with respect to strains. Stretching the rubber composite increases the efficiency due to the increase in entropic force (rubber elasticity)[63]. Maximum energy conversion efficiencies of ~0.0045% was measured, which is ~50 times larger than reported photo-thermal (8.5 x 10-5%) efficiencies for PVDF polymer based light driven actuators[62]. These numbers are also in the same range to recently reported energy conversion efficiencies of ~0.003% for graphene based photo-mechanical actuators[64].

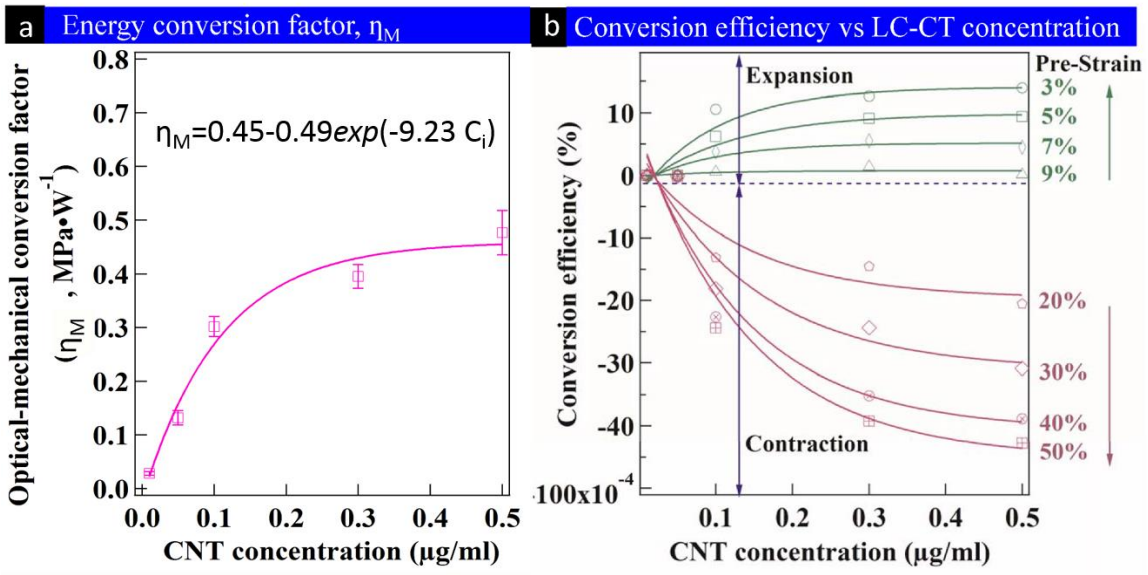

Figure 4.12 | Efficiencies of nanotube LC-polymer composites: (a) Opto-mechanical conversion factor versus concentration; (b) Energy conversion efficiency versus concentration at different pre-strains.

Figure 4. 13 presents the nanotube mass fractions comparing our layered LC photo-mechanical actuators to all other nanocomposite photomechanical actuators employing nanotubes and polymers and reported till date in this area[12, 13, 42, 51, 52, 65]. Past reported nanotube/graphene based nanocomposite photomechanical actuators have used anywhere from ~0.02 wt.% to ~7 wt.% of nanotubes and 0-5 wt.% of graphene in PDMS respectively[12, 13, 42, 51, 52, 65]. These are randomly oriented nanotube/graphene mixed inside the polymers as nanocomposites and do not show any optical anisotropy. Even after stretching no liquid crystal ordering was seen in the past actuators. The mass of CNT used in these past actuators for the wt.% mentioned above correspond to ~22 μg-1100 μg of nanotube/graphene used to prepare the composites [12, 13, 42, 51, 52, 65]. Compared to that the present LC films reported here use only ~0.07-3.31 μg of CNT mass which is ~100-10,000 times smaller.

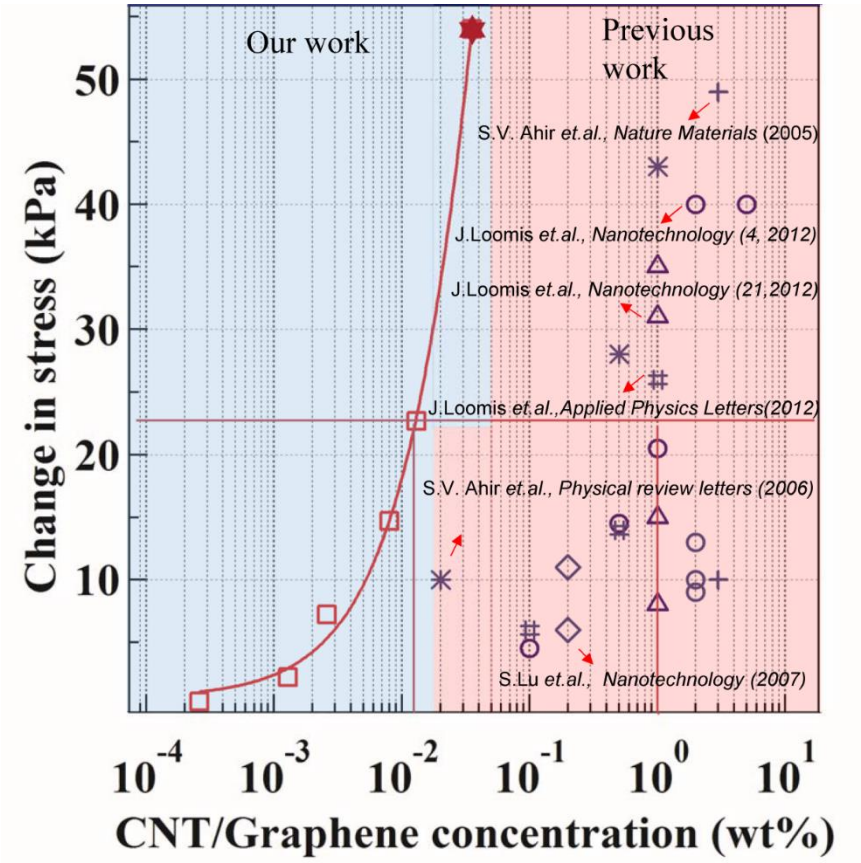

Figure 4.13 | Stress versus Mass Fractions Comparisons: Logarithmic plot of mass fractions of CNT/graphene versus stress suggesting superior performance of nanotube LC elastomers compared to previous nanotube/graphene based nanocomposite photomechanical actuators. It should be noted that the present work has a layered composite structure unlike most past studies which were nanocomposites.

CHAPTER 5

CONCLUSIONS

This study presents novel composite system consisting of nanotube LCs in elastomers and their performance as light driven actuators. The work combines the anisotropic properties of LCs with flexibility of elastomers which has been the approach for photo-chromic actuators in the past[66]. This work also demonstrates the use of ultra-small amounts of nanotubes to achieve a large mechanical response compared to past reported actuators in this area till date[12, 42, 52, 64, 65]. The actuator in this study is a laminate with 2 layers of PDMS in between self-assembled nanotube LC layer. So while this is different design from a nanocomposite, the amount of high quality nanotube used is significantly smaller for the same response. 1 mg/100 ml of >99% purity nanotubes today costs ~$799. The 47 mm anodisc film/85 mm film on MCE filter membrane as reported here and in the recent past needs 1 ml of nanotube stock solution. We have been able to make 100 films (30-35 mm in anodisc) using the 100 ml stock solution. Each LC film resulted in 5-10 actuators of the size mentioned. Therefore, one can make anywhere between 500-1000 actuators using 100 ml nanotube stock solution, which cost anywhere between $0.80 to $1.50 approximately. Since there is no additional processing for aligning the nanotubes, these films may be highly useful for applications such as thin film transistors with high electron mobility[67] and nanopositioning systems at low cost[64].

The transfer process and the ability to define composites with specific order parameters and relate them to concentration, elastic modulus and photomechanical response could be useful for making standardized nanotube composites based on LCs. Lack of standard processing techniques of carbon nanotube composites have hindered commercialization and the present work shows a novel pathway consisting of simple and low cost vacuum filtration followed by transfer process which preserves the orientation of the LC. The present work could also be of significant interest to electro-mechanical actuation technologies and creating artificial muscles with other polymers employing our processing technique, where high anisotropic SWNT conductivity and percolation pathways are preferred. In the past, large amounts of SWNT was required (almost 0.1-18% w/w in nafion of randomly oriented HiPco nanotubes[14]) to achieve high conductivity and subsequent electro-mechanical actuation (macroscopic response of 4.5 mm at 18% w/w SWNT). This makes them prohibitively expensive. Compared to this, our nanotube LC actuators use four orders of magnitude small mass fractions of nanotube. Electro-mechanical actuators and energy conversion devices based on low mass fractions using nanotube LCs could pave the way for commercial development. It is seen that with increasing concentration, the domain size decreases and use of polarization microscopy to image dichroic nanotubes is convenient for creating map of domain size and their counts. In this case, the domain size indicates the size of the aligned carbon nanotubes against a specific director. These domains might be highly interesting in studies concerning strains in composites and their non-destructive evaluation based on polarization microscopy. Manufacturing nanotube LC composites with specific order could also mean specific physical properties thereby enabling standardization of nanotube-polymer composite

manufacturing processes. Eliminating process complexities such as acid treatment and functionalization of nanotubes in polymer composites thus makes our process environmentally benign. It may be possible that structural laminates based on epoxies could use LC nanotubes as fillers enabling super strong composites with order dependent mechanical properties.

Commercial polymers such as polyvinylidene fluoride (PVDF) have calculated opto-mechanical conversion factor (η_m) of ~97 $kPaW^{-1}$ is 5 times smaller than the value of ~0.5 $MPaW^{-1}$ reported for nanotube-LC actuators. Further, the energy conversion efficiencies were ~50 times larger (8.5 x 10^{-5}% for PVDF versus 0.0045% for nanotube-LC) compared to PVDF[62]. Polymers containing cinnamic groups were reported to be deformed and fixed into pre-determined shapes such as elongated films and tubes, arches or spirals by ultraviolet light illumination. However, they can only be recovered to their original shape by irradiating UV light of different wavelength for 60 minutes[68]. Compared to this the nanotube LC actuators relax to their original configuration after light is switched off and are thus reversible. The strain dependent energy conversion would also be useful in energy scavenging using vibrational effects. Nanotube LC actuators as presented here show optical anisotropy, unique photomechanical response and tunable energy conversion in one system making this important for smart applications.

REFERENCES

[1] P.-G. De Gennes and J. Prost, *The physics of liquid crystals* vol. 23: Clarendon press Oxford, 1993.

[2] K. Namba and G. Stubbs, "Structure of tobacco mosaic virus at 3.6 A resolution: implications for assembly," *Science,* vol. 231, pp. 1401-1406, 1986.

[3] H. Schröder, "Aggregation of proteins in membranes. An example of fluctuation-induced interactions in liquid crystals," *The Journal of Chemical Physics,* vol. 67, pp. 1617-1619, 1977.

[4] A. Lazaris, S. Arcidiacono, Y. Huang, J.-F. Zhou, F. Duguay, N. Chretien*, et al.*, "Spider silk fibers spun from soluble recombinant silk produced in mammalian cells," *Science,* vol. 295, pp. 472-476, 2002.

[5] T. Thompson and T. W. Tillack, "Organization of glycosphingolipids in bilayers and plasma membranes of mammalian cells," *Annual review of biophysics and biophysical chemistry,* vol. 14, pp. 361-386, 1985.

[6] Y. Ide and Z. Ophir, "Orientation development in thermotropic liquid crystal polymers," *Polymer Engineering & Science,* vol. 23, pp. 261-265, 1983.

[7] T. Kato, "Self-assembly of phase-segregated liquid crystal structures," *Science,* vol. 295, pp. 2414-2418, 2002.

[8] V. Vorflusev and S. Kumar, "Phase-separated composite films for liquid crystal displays," *Science,* vol. 283, pp. 1903-1905, 1999.

[9] W. Song, I. A. Kinloch, and A. H. Windle, "Nematic liquid crystallinity of multiwall carbon nanotubes," *Science,* vol. 302, pp. 1363-1363, 2003.

[10] B. King and B. Panchapakesan, "Vacuum filtration based formation of liquid crystal films of semiconducting carbon nanotubes and high performance transistor devices," *Nanotechnology,* vol. 25, p. 175201, 2014.

[11] H. Koerner, G. Price, N. A. Pearce, M. Alexander, and R. A. Vaia, "Remotely actuated polymer nanocomposites—stress-recovery of carbon-nanotube-filled thermoplastic elastomers," *Nature materials,* vol. 3, pp. 115-120, 2004.

[12] S. V. Ahir and E. M. Terentjev, "Photomechanical actuation in polymer–nanotube composites," *Nature materials,* vol. 4, pp. 491-495, 2005.

[13] J. Loomis, B. King, T. Burkhead, P. Xu, N. Bessler, E. Terentjev, *et al.*, "Graphene-nanoplatelet-based photomechanical actuators," *Nanotechnology,* vol. 23, p. 045501, 2012.

[14] B. J. Landi, R. P. Raffaelle, M. J. Heben, J. L. Alleman, W. VanDerveer, and T. Gennett, "Single wall carbon nanotube-Nafion composite actuators," *Nano Letters,* vol. 2, pp. 1329-1332, 2002.

[15] G. J. White and R. Padman, "Images of atomic carbon in the interstellar medium," 1991.

[16] T. Henning and F. Salama, "Carbon in the Universe," *Science,* vol. 282, pp. 2204-2210, 1998.

[17] A. Hirsch, "The era of carbon allotropes," *Nature materials,* vol. 9, pp. 868-871, 2010.

[18] H. W. Kroto, J. R. Heath, S. C. O'Brien, R. F. Curl, and R. E. Smalley, "C 60: buckminsterfullerene," *Nature,* vol. 318, pp. 162-163, 1985.

[19] S. Iijima, "Helical microtubules of graphitic carbon," *nature,* vol. 354, pp. 56-58, 1991.

[20] K. S. Novoselov, A. K. Geim, S. Morozov, D. Jiang, Y. Zhang, S. Dubonos, *et al.*, "Electric field effect in atomically thin carbon films," *science,* vol. 306, pp. 666-669, 2004.

[21] G. G. Tibbetts, "Why are carbon filaments tubular?," *Journal of crystal growth,* vol. 66, pp. 632-638, 1984.

[22] D. Bethune, C. Klang, M. De Vries, G. Gorman, R. Savoy, J. Vazquez, *et al.*, "Cobalt-catalysed growth of carbon nanotubes with single-atomic-layer walls," 1993.

[23] S. Iijima and T. Ichihashi, "Single-shell carbon nanotubes of 1-nm diameter," 1993.

[24] R. S. Ruoff and D. C. Lorents, "Mechanical and thermal properties of carbon nanotubes," *carbon,* vol. 33, pp. 925-930, 1995.

[25] J. Mintmire, B. Dunlap, and C. White, "Are fullerene tubules metallic?," *Physical Review Letters,* vol. 68, p. 631, 1992.

[26] C. Dekker, "Carbon nanotubes as molecular quantum wires," *Physics today,* vol. 52, pp. 22-30, 1999.

[27] M.-F. Yu, O. Lourie, M. J. Dyer, K. Moloni, T. F. Kelly, and R. S. Ruoff, "Strength and breaking mechanism of multiwalled carbon nanotubes under tensile load," *Science,* vol. 287, pp. 637-640, 2000.

[28] Y.-C. Tseng, P. Xuan, A. Javey, R. Malloy, Q. Wang, J. Bokor*, et al.*, "Monolithic integration of carbon nanotube devices with silicon MOS technology," *Nano Letters,* vol. 4, pp. 123-127, 2004.

[29] D. Janas, A. P. Herman, S. Boncel, and K. K. Koziol, "Iodine monochloride as a powerful enhancer of electrical conductivity of carbon nanotube wires," *Carbon,* vol. 73, pp. 225-233, 2014.

[30] S. Ng, J. Wang, Z. Guo, J. Chen, G. Wang, and H. K. Liu, "Single wall carbon nanotube paper as anode for lithium-ion battery," *Electrochimica Acta,* vol. 51, pp. 23-28, 2005.

[31] G. K. Mor, K. Shankar, M. Paulose, O. K. Varghese, and C. A. Grimes, "Use of highly-ordered TiO2 nanotube arrays in dye-sensitized solar cells," *Nano letters,* vol. 6, pp. 215-218, 2006.

[32] A. Dillon, K. Jones, T. Bekkedahl, C. Kiang, D. Bethune, and M. Heben, "Storage of hydrogen in single-walled carbon nanotubes," *Nature,* vol. 386, pp. 377-379, 1997.

[33] D. N. Futaba, K. Hata, T. Yamada, T. Hiraoka, Y. Hayamizu, Y. Kakudate*, et al.*, "Shape-engineerable and highly densely packed single-walled carbon nanotubes and their application as super-capacitor electrodes," *Nature materials,* vol. 5, pp. 987-994, 2006.

[34] H. Lin, H. Zhu, H. Guo, and L. Yu, "Investigation of the microwave-absorbing properties of Fe-filled carbon nanotubes," *Materials Letters,* vol. 61, pp. 3547-3550, 2007.

[35] E. J. Petersen, X. Tu, M. Dizdaroglu, M. Zheng, and B. C. Nelson, "Protective Roles of Single-Wall Carbon Nanotubes in Ultrasonication-Induced DNA Base Damage," *Small,* vol. 9, pp. 205-208, 2013.

[36] C. Mavroidis, C. Pfeiffer, and M. Mosley, "Conventional actuators, shape memory alloys, and electrorheological fluids."

[37] M. H. Li, P. Keller, B. Li, X. Wang, and M. Brunet, "Light-Driven Side-On Nematic Elastomer Actuators," *Advanced Materials,* vol. 15, pp. 569-572, 2003.

[38] D. H. Wang, K. M. Lee, Z. Yu, H. Koerner, R. A. Vaia, T. J. White*, et al.*, "Photomechanical response of glassy azobenzene polyimide networks," *Macromolecules,* vol. 44, pp. 3840-3846, 2011.

[39] S. S. Sarkisov, M. J. Curley, A. Fields, S. S. Sarkisov II, and G. Adamovsky, "Photomechanical effect in films of polyvinylidene fluoride," *Applied physics letters,* vol. 85, pp. 2747-2749, 2004.

[40] A. V. Srinivasan and D. M. McFarland, *Smart structures: analysis and design*: Cambridge university press, 2001.

[41] M. Stuchlik, P. Kreemer, and S. Elliott, "Opto-mechanical effect in chalcogenide glasses," DTIC Document2001.

[42] S. Lu and B. Panchapakesan, "Photomechanical responses of carbon nanotube/polymer actuators," *Nanotechnology,* vol. 18, p. 305502, 2007.

[43] S. Chandrasekhar, B. Sadashiva, and K. Suresh, "Liquid crystals of disc-like molecules," *pramana,* vol. 9, pp. 471-480, 1977.

[44] J. P. Lagerwall and G. Scalia, "Carbon nanotubes in liquid crystals," *Journal of Materials Chemistry,* vol. 18, pp. 2890-2898, 2008.

[45] S. Badaire, C. Zakri, M. Maugey, A. Derré, J. N. Barisci, G. Wallace*, et al.*, "Liquid crystals of DNA-stabilized carbon nanotubes," *Advanced Materials,* vol. 17, pp. 1673-1676, 2005.

[46] C. Zakri, "Carbon nanotubes and liquid crystalline phases," *Liquid Crystals Today,* vol. 16, pp. 1-11, 2007.

[47] V. A. Davis, L. M. Ericson, A. N. G. Parra-Vasquez, H. Fan, Y. Wang, V. Prieto*, et al.*, "Phase behavior and rheology of SWNTs in superacids," *Macromolecules,* vol. 37, pp. 154-160, 2004.

[48] Q. Li, Y. T. Zhu, I. A. Kinloch, and A. H. Windle, "Self-organization of carbon nanotubes in evaporating droplets," *The Journal of Physical Chemistry B,* vol. 110, pp. 13926-13930, 2006.

[49] C. Zakri and P. Poulin, "Phase behavior of nanotube suspensions: from attraction induced percolation to liquid crystalline phases," *Journal of Materials Chemistry,* vol. 16, pp. 4095-4098, 2006.

[50] E. Hobbie and D. Fry, "Nonequilibrium phase diagram of sticky nanotube suspensions," *Physical review letters,* vol. 97, p. 036101, 2006.

[51] J. Loomis and B. Panchapakesan, "Dimensional dependence of photomechanical response in carbon nanostructure composites: a case for carbon-based mixed-dimensional systems," *Nanotechnology,* vol. 23, p. 215501, 2012.

[52] J. Loomis, B. King, and B. Panchapakesan, "Layer dependent mechanical responses of graphene composites to near-infrared light," *Applied Physics Letters,* vol. 100, p. 073108, 2012.

[53] H. Peng, L. B. Alemany, J. L. Margrave, and V. N. Khabashesku, "Sidewall carboxylic acid functionalization of single-walled carbon nanotubes," *Journal of the American Chemical Society,* vol. 125, pp. 15174-15182, 2003.

[54] T. Ramanathan, A. Abdala, S. Stankovich, D. Dikin, M. Herrera-Alonso, R. Piner*, et al.*, "Functionalized graphene sheets for polymer nanocomposites," *Nature nanotechnology,* vol. 3, pp. 327-331, 2008.

[55] W. Guo and B. Fung, "Determination of the order parameters of liquid crystals from carbon-13 chemical shifts," *The Journal of chemical physics,* vol. 95, pp. 3917-3923, 1991.

[56] C. A. Schneider, W. S. Rasband, K. W. Eliceiri, J. Schindelin, I. Arganda-Carreras, E. Frise*, et al.*, "NIH image to imageJ: 25 years of image analysis," *Nature methods,* vol. 9, 2012.

[57] T. Ramanathan, H. Liu, and L. Brinson, "Functionalized SWNT/polymer nanocomposites for dramatic property improvement," *Journal of Polymer Science Part B: Polymer Physics,* vol. 43, pp. 2269-2279, 2005.

[58] D. Cai, A. Neyer, R. Kuckuk, and H. Heise, "Optical absorption in transparent PDMS materials applied for multimode waveguides fabrication," *Optical materials,* vol. 30, pp. 1157-1161, 2008.

[59] G. Williams and D. C. Watts, "Non-symmetrical dielectric relaxation behaviour arising from a simple empirical decay function," *Transactions of the Faraday Society,* vol. 66, pp. 80-85, 1970.

[60] M. Potuzak, R. C. Welch, and J. C. Mauro, "Topological origin of stretched exponential relaxation in glass," *The Journal of chemical physics,* vol. 135, p. 214502, 2011.

[61] S. Ahir and E. Terentjev, "Fast relaxation of carbon nanotubes in polymer composite actuators," *Physical review letters,* vol. 96, p. 133902, 2006.

[62] S. S. Sarkisov, M. J. Curley, G. Adamovsky, L. Huey, and A. Fields, "Light-driven actuators based on polymer films," *Optical Engineering,* vol. 45, pp. 034302-034302-10, 2006.

[63] L. H. Sperling, *Introduction to physical polymer science*: John Wiley & Sons, 2005.

[64] J. Loomis, X. Fan, F. Khosravi, P. Xu, M. Fletcher, R. W. Cohn*, et al.*, "Graphene/elastomer composite-based photo-thermal nanopositioners," *Scientific reports,* vol. 3, 2013.

[65] S. Ahir, A. Squires, A. Tajbakhsh, and E. Terentjev, "Infrared actuation in aligned polymer-nanotube composites," *Physical review B,* vol. 73, p. 085420, 2006.

[66] J.-i. Mamiya, "Photomechanical energy conversion based on cross-linked liquid-crystalline polymers," *Polymer Journal,* vol. 45, pp. 239-246, 2012.

[67] P. H. Lau, K. Takei, C. Wang, Y. Ju, J. Kim, Z. Yu*, et al.*, "Fully printed, high performance carbon nanotube thin-film transistors on flexible substrates," *Nano letters,* vol. 13, pp. 3864-3869, 2013.

[68] A. Lendlein, H. Jiang, O. Jünger, and R. Langer, "Light-induced shape-memory polymers," *Nature,* vol. 434, pp. 879-882, 2005.

CURRICULUM VITA

Xiaoming Fan

2239 Arthur Ford Ct.

Louisville, KY 40217

anyonefxm@gmail.com

Tel: 502-468-6922

I. Education

Master of Science in Mechanical Engineering, August 2014

JB Speed School of Engineering, University of Louisville, Louisville, KY, USA

Thesis topic: Photo Mechanical Actuation of Liquid Crystal Nanotube Elastomers

Bachelor of Engineering in Polymer Materials and Engineering, June 2007

College of Materials Science and Engineering, Beijing University of Chemical Technology, Beijing, China

Thesis topic: Collagen Cerium Complexes' Preparation and the Research on Its Antimicrobial Property.

II. Experience

Graduate Research Assistant, April 2013 - Present

Small Systems Laboratory, 221 Shumaker Research Building, University of Louisville, Louisville, KY, USA

Research Consultant, March 2008 - May 2011

China National Chemical Information Center, No. 53, Xiaoguanjie, Chaoyang District, Beijing, China

Vice manager of Oversea Sale & Marketing, May 2011 – July 2012

China National Chemical Information Center, No. 53, Xiaoguanjie, Chaoyang District, Beijing, China

III. Skills and Coursework

Materials Characterization: Scanning Electron Microscopy (SEM), AFM, Raman spectroscopy, X-ray Photo-electron Spectroscopy (XPS), Polarized microscopy

Micro/nano technology fabrication: Carbon nanotube film deposition

Mechanical text: Stress-strain test, photomechanical stress test

High level programming: Origin, Igor Pro, LabView, Solidworks

Select Courses:

Introduction to Micro/Nano Technology

Optimum Method Design

Finite Elements Method Mechanical Design I

Foundation of Microfabrication and MEMS

Material Characterization\

Fiber Reinforcement Composites

IV. Publications

- J. Loomis, X. Fan, F. Khosravi, P. Xu, M. Fletcher, R.W. Cohn and B. Panchapakesan, "Graphene/elastomer composite-based photo-thermal nanopositioners, 2013 Scientific Reports 3, 1900, NATURE Publishing Group (NPG).
- Xiaoming Fan, et al. Nanotube Liquid Crystal Elastomers: Photomechanical Response and Flexible Energy Conversion of Layered Polymer Composites, Nanotechnology, in progress